

Seismic Fragility of Italian Code-Conforming Buildings by Multi-Stripe Dynamic Analysis of Three-Dimensional Structural Models

Iunio Iervolino, Roberto Baraschino, Andrea Belleri, Donatello Cardone, Gaetano Della Corte, Paolo Franchin, Sergio Lagomarsino, Gennaro Magliulo, Andrea Marchi, Andrea Penna, Luciano R.S. Viggiani & Alessandro Zona

To cite this article: Iunio Iervolino, Roberto Baraschino, Andrea Belleri, Donatello Cardone, Gaetano Della Corte, Paolo Franchin, Sergio Lagomarsino, Gennaro Magliulo, Andrea Marchi, Andrea Penna, Luciano R.S. Viggiani & Alessandro Zona (2023) Seismic Fragility of Italian Code-Conforming Buildings by Multi-Stripe Dynamic Analysis of Three-Dimensional Structural Models, *Journal of Earthquake Engineering*, 27:15, 4415-4448, DOI: [10.1080/13632469.2023.2167889](https://doi.org/10.1080/13632469.2023.2167889)

To link to this article: <https://doi.org/10.1080/13632469.2023.2167889>



Published online: 01 Feb 2023.



Submit your article to this journal [↗](#)



Article views: 353



View related articles [↗](#)



View Crossmark data [↗](#)



Citing articles: 1 View citing articles [↗](#)



Seismic Fragility of Italian Code-Conforming Buildings by Multi-Stripe Dynamic Analysis of Three-Dimensional Structural Models

Iunio Iervolino ^a, Roberto Baraschino ^a, Andrea Belleri ^b, Donatello Cardone ^c, Gaetano Della Corte ^a, Paolo Franchin ^d, Sergio Lagomarsino ^e, Gennaro Magliulo ^a, Andrea Marchi ^d, Andrea Penna ^f, Luciano R.S. Viggiani ^e, and Alessandro Zona ^g

^aDipartimento di Strutture per l'Ingegneria e l'Architettura, Università degli Studi di Napoli Federico II, Naples, Italy;

^bDipartimento di Ingegneria e Scienze Applicate, Università degli Studi di Bergamo, Bergamo, Italy; ^cScuola di Ingegneria, Università degli Studi della Basilicata, Potenza, Italy; ^dDipartimento di Ingegneria Strutturale e Geotecnica, Sapienza Università di Roma, Rome, Italy; ^eDipartimento di Ingegneria Civile, Chimica e Ambientale, Università degli Studi di Genova, Genova, Italy; ^fCentro Europeo di Formazione e Ricerca in Ingegneria Sismica (EUCENTRE), Pavia, Italy; ^gScuola di Architettura e Design, Università degli Studi di Camerino, Camerino, Italy

ABSTRACT

The RINTC (2015–2017) project was a three-year research program aimed at assessing the seismic reliability of code-conforming structures in Italy. It dealt with five structural typologies of residential and industrial buildings: reinforced concrete, masonry, precast reinforced concrete, steel, and base isolated reinforced concrete. To reach its goals, several tens of structures featuring the same configuration were designed at different sites, characterized by different seismic hazard and considering two soil site conditions. The failure risk (i.e. the failure rate) of the buildings was evaluated by means of non-linear dynamic analysis of three-dimensional numerical models. The study herein presented parametrized the vulnerability models of the considered structures; in other words, it provides the seismic fragility curves for code-conforming Italian buildings analyzed in the RINTC project. Lognormal fragilities refer to global collapse failure and usability preventing damage, which are the performances considered in the project, and are derived via state-of-the-art methods, including consideration of the uncertainty in the estimation of their parameters. The curves are made available to be possibly used for further risk analyses and enable a discussion of the fragility fitting issues as a function on the site's hazard.

ARTICLE HISTORY

Received 26 March 2022
Accepted 8 January 2023

KEYWORDS

Failure rate; reliability; probabilistic seismic hazard analysis; performance-based earthquake engineering; seismic risk

Introduction

In the current Italian building code (NTC hereafter; CS.LL.PP. 2008, 2018), somewhat similar to Eurocode 8 or EC8 (CEN 2004), structural performance must be verified with respect to seismic action (i.e. the ground motion intensity) with specific return periods (T_R) of exceedance at the site of interest. The design return period depends on the *limit state* considered for design; for example, in case of *ordinary* (e.g. office or residential) structures, safety verifications for damage and life safety limit states are required against ground motion intensity measure (IM) levels corresponding to T_R of 50 and 475 years, respectively. However, although such design intensities have a probabilistic determination, seismic structural reliability resulting by design is not explicitly controlled.

To quantitatively address the seismic risk that the code-conforming design exposes structures to, a large research project was conducted in Italy between 2015 and 2017 (with some continuation in 2018). In the project, named *Rischio Implicito – Norme Tecniche per le Costruzioni* or RINTC (RINTC-

Workgroup 2018), structures belonging to a variety of structural types, that is, un-reinforced masonry (URM); reinforced concrete (RC), precast reinforced concrete (PRC), steel (S), and base isolated reinforced concrete buildings (BI), was designed according to NTC. The buildings are for residential and industrial occupancy, and various architectural/structural configurations were considered for each typology. Three sites, featuring different hazard levels (Milan, Naples, and L'Aquila), and two local site conditions (soil types A and C, according to the EC8 classification), were considered (Iervolino and Dolce 2018). The seismic structural reliability of the designed structures was assessed in terms of annual failure rate of *global collapse* (GC) and *usability-preventing damage* (UPD). The rates were computed within the performance-based earthquake engineering (PBEE) framework (Cornell and Krawinkler 2000), that is, integrating the seismic structural fragility and the hazard curve for the design site.

In the RINTC project, structural fragility was only obtained as conditional (lumped) probabilities at ten IM levels, and fragility curves were not fitted (Iervolino, Spillatura, and Bazzurro 2018). On the other hand, parametric fragility curves of the several buildings designed, modeled, and analyzed in the RINTC project can be useful for a critical discussion of the vulnerability of code-conforming structures and for further risk assessment studies. This motivated the study presented herein, where hundreds of hazard-consistent seismic fragility curves are provided for the models belonging to the five structural typologies and both failure criteria investigated in the project.

Among the variety of approaches to derive a fragility function, the study herein presented focuses on so-called non-linear dynamic analysis of three-dimensional (3D) models. In particular, the results of the multiple-stripe analysis or MSA (Jalayer and Cornell 2003), using hazard-consistent ground motion record sets, are used to fit lognormal fragility curves for the RINTC structures at all the sites design refers to. The curves are obtained considering a variety of procedures able to manage the numerical instabilities arising from non-linear dynamic analysis and/or the cases of low-hazard sites, where failures are rarely observed. Moreover, the uncertainty in estimation (Iervolino 2017) of the fragility parameters, arising from the *record-to-record variability* of structural response (Shome et al. 1998), is also addressed. This study is consistent with results of previous work based on equivalent single-degree-of-freedom (ESDoF) approximation (Suzuki and Iervolino 2021); however, it represents an advancement, not only for the fragility derivation based on 3D modeling, but also because the fragility via ESDoF were only evaluated for a small subset of cases with respect to those addressed herein.

The remainder of the paper is structured such that the results of the RINTC project are briefly recalled first. Then three methods for lognormal fragility fitting are discussed. Subsequently the parametric fragility curves are presented. As a validation of the fragilities, the failure rates computed via the fitted curves are compared with those evaluated within the RINTC project and differences are quantitatively explained. Some final remarks close the paper.

The RINTC Framework

Life Safety and Damage Design

According to the NTC, seismic design actions derive from probabilistic seismic hazard analysis or PSHA (Cornell 1968). Structural systems must withstand those with the return period of exceedance depending on the limit state of interest at the construction site. For ordinary structures, mandatory design limit states are *damage* (SLD) and *life safety* (SLV). They correspond to design shaking intensity, on rock site conditions, defined in terms of 5% damped spectral pseudo-accelerations, $Sa_{SLD}(T)$ and $Sa_{SLV}(T)$ (where T is the natural vibration period), taken from site-specific elastic spectra that are close approximations of the 50 and 475 year return period uniform hazard spectra (UHS). Soil conditions are accounted for via soil-class-specific modification factors.

Fig. 1a shows the Italian seismic hazard map, currently considered by NTC, in terms of peak ground acceleration (PGA) with 475-year return period of exceedance on rock. The three considered

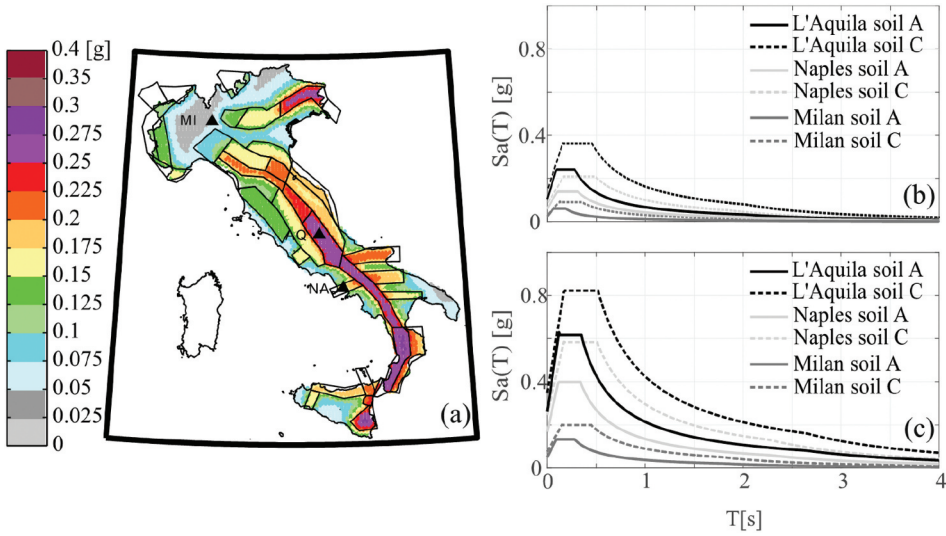


Figure 1. (a) Italian seismic source zones and corresponding hazard map in terms of PGA with 475-year exceedance return period on rock; (b) elastic design spectra corresponding to 50-year return period and (c) 475-year return period for the considered sites.

design sites, representative of low-, mid- and high-hazard in the country, indicated as MI (Milan), NA (Naples), and AQ (L'Aquila), respectively, are also shown in the figure.

Fig. 1b, c shows the design spectra at the sites for the two soil site conditions (A and C according to the EC8 classification), for the two considered design limit states. If linear analysis is employed for design, the code allows to introduce a *behavior factor* (q) to obtain inelastic design spectra. Those assumed in the project are recalled in the next section for each typology.

Residential URM Buildings

URM buildings are two- or three-story buildings made of perforated clay units with mortar joints. Different architectural configurations, either regular or irregular, according to the definition provided by NTC, were considered as to represent typical Italian residential buildings: regular configurations are indicated as C (C1-C7), E2, E8, E9, while those irregular as I, E5 (see Cattari et al. 2018; Manzini et

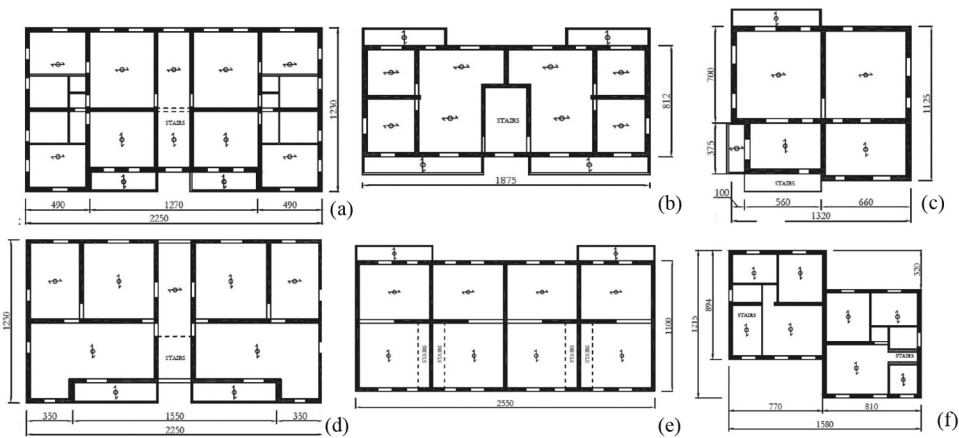


Figure 2. URM plan configurations: (a) C, (b) E2, (c) E5, (d) E8, (e) E9, (f) I.

al. 2018, for design and modeling details). As an example, Fig. 2a shows the plan of a C-type configuration building; Fig. 2b, Fig. 2d, e shows the plan of the E2, E8 and E9 buildings; Fig. 2c, f shows the plan of the E5 and I configurations.

The applied design methods are: *simple building* (SB) rules, *linear static analysis* (with equivalent frame, LSA-F, or with cantilever modeling, LSA-C), and *non-linear static analysis* (NLSA). In case of LSA, design seismic action was determined by the elastic response spectra divided by a behavior factor q equal to 3.6.

The building-site combinations examined in this study are listed via the following code format, TYPOLOGY-CONFIGURATION-STOREY-SITE-SOIL*, where the typology is URM; the configuration can take one among C1, C7, E2, E8, E9, I, E5, values, story is either 2 or 3, design site is AQ, NA, or MI, and soil is A or C. Finally, the (eventual) asterisk indicates design according to the recent update of NTC (CS.LL.PP. 2018).

Residential RC Buildings

Three-, six-, and nine-story RC moment-resisting frame (MRF) buildings, and nine-story RC shear walls (SW) buildings were designed. Some cases include soil-structure interaction (SSI) and modeling uncertainty (MU) (RINTC-Workgroup 2018; Franchin et al. 2018), but they were not considered in the fragility derivation herein.

The buildings were intended for residential use and are all 5×3 bays, characterized by regularity in plan (e.g. Fig. 3d) and elevation. The floor area is approximately $21.4 \times 11.7\text{m}^2$, for all. The ground floor height and all other story heights are 3.4m and 3.05m , respectively. The RC frames include knee-joint beams designed to support the staircases.

Three different structural configurations, that is, bare-, infilled-, and *pilotis*-frames, hereafter denoted as BF, IF, and PF, respectively (Fig. 3a–c), were considered. The structural members of BF and IF are identical in dimensions and reinforcement detailing, while the vertical structural members at the ground floor of PF were strengthened to account for the infill reduction. SW buildings have walls symmetrically arranged along the perimeter; the walls are 35cm thick with section height varying with site and kept for three consecutive floors (plan view in Fig. 3e).

For each site, seismic design was performed by means of *modal response spectrum* (MRS) analysis. The reference design strength was assigned applying a behaviour factor $q = 3.9$ to the horizontal

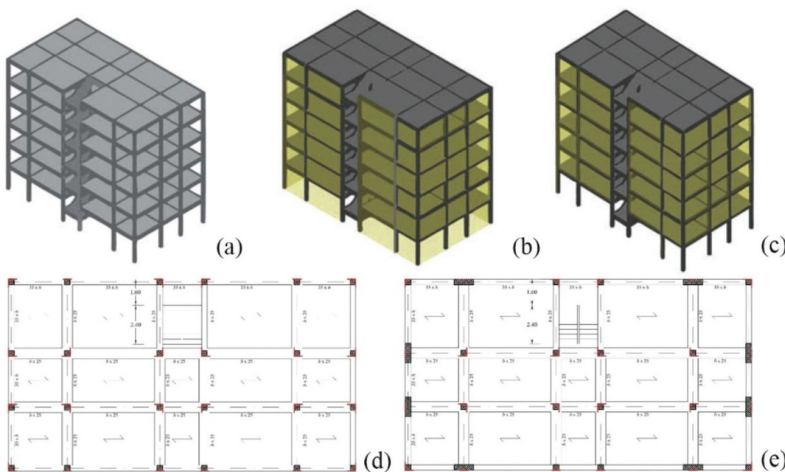


Figure 3. (a) six story bare-frame (BF); (b) six story infilled-frame (IF); (c) six story pilotis-frame (PF); (d) MRF building floor plan; (e) SW building floor plan.

elastic response spectrum (Fig. 1c), which means to consider RC frames in *low-ductility* class, corresponding to the medium ductility class in EC8; see Ricci et al. (2018) for details.

The structures considered herein are listed via the following code format `TYPOLOGY-SHEAR_WALLS_PRESENCE-STOREY-INFILLINGS_CONFIGURATION-STOREYS-SITE-SOIL`, where the typology is RC, the possible presence of shear walls is indicated as SW, the infillings configuration can be BF-PF-IF, story is 3, 6, or 9, design site is AQ, NA, or MI, and soil is A or C.

BI Reinforced Concrete Buildings

A series of RC isolated buildings was designed, where the superstructure is the six-story MRF, the plan view of which is shown in Fig. 3d. Three different isolation systems were considered: double-curvature friction pendulums (FPS), high-damping rubber bearings (HDRB), and a hybrid system made of HDRBs and sliders (SLDR). Buildings were designed only for mid- and high-hazard sites (Naples and L'Aquila), on soil C. The seismic response of isolated buildings has been evaluated by accounting for the non-linear behaviour of both the isolation system and the superstructure; see Ragni et al. (2018), Micozzi et al. (2021), and Ponzo et al. (2021).

The six structures considered are listed in the following code format, `TYPOLOGY-ISOLATION_SYSTEM-SITE-SOIL`, where the typology is BI, the isolation system can be FPS, HDRB, or HDRB+SLD, design site is AQ or NA, and soil is C.

Industrial PRC Buildings

Single-story industrial PRC buildings were designed at the three sites. Each building features 4×1 bays, with precast columns and prestressed principal beams, longitudinal gutter beams, prestressed roof elements, and vertical/horizontal cladding. The principal beams have varying cross-sections and height, while columns are rectangular. Fig. 4a, b shows the plan and elevation views of the prototype buildings, respectively. The columns were assumed to have pocket foundations and connected at the top, to both the transverse and longitudinal beams, through dowel connections. The roof system consists of precast elements, which are pinned to the beams by means of dowel connections and connected to each other by steel elements in conjunction with a cast-in-situ concrete slab ensuring a roof rigid diaphragm behaviour. The vertical cladding panels are connected to the beams and columns by means of steel connections. The travelling crane, typical of industrial buildings, was not modeled in the analysis, but accounted for in the design via corbels in the columns to support steel runway beams.

For each site, four different configurations were considered, varying four geometry parameters of the frames. Those parameters are summarized in Table 1, where transverse and longitudinal bay widths and story- and crane-bracket heights are indicated as L_x , L_y , H , and H_c respectively.

MRS analysis, for the horizontal and vertical directions at each site, was applied for design. The design spectrum was obtained from the horizontal elastic response spectra (Fig. 1c) considering a

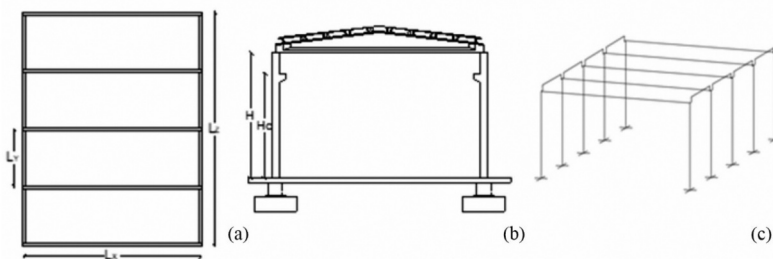


Figure 4. Prototype PRC buildings in plan view (a), transversal frame (b), and numerical model (c).

Table 1. Geometry parameters for the prototype PRC buildings.

| Geometry | L_x [m] | L_y [m] | H [m] | H_c [m] |
|----------|-----------|-----------|---------|-----------|
| Geom1 | 15 | 6 | 6 | 4.5 |
| Geom2 | 20 | 8 | 6 | 4.5 |
| Geom3 | 15 | 6 | 9 | 7.5 |
| Geom4 | 20 | 8 | 9 | 7.5 |

behaviour factor $q = 2.5$ that applies to low-ductility class precast buildings with isostatic columns according to NTC (Gajera et al. 2021; Magliulo, Di Salvatore, and Ercolino 2021; Magliulo et al. 2018).

The resulting twenty-four structures are enumerated via the following code format TYPOLOGY-GEOMETRY-SITE-SOIL, where the typology is PRC, geometry can be GEOM-1, 2, 3, or 4, design site is AQ, NA or MI, and soil is A or C.

Industrial Steel Buildings

Single-story industrial steel buildings equipped with an overhead travelling crane were designed; i.e. four geometries in the three considered sites each considering the soil conditions, A and C. As shown in Fig. 5, the prototype buildings are made of five equally spaced transverse single-span duo-pitch portal frames connected through longitudinal beams at the apex, eaves, and crane-supporting bracket levels. Lateral loads are sustained by the MRF system in the transverse direction while the resistance in the longitudinal direction is assigned to diagonal concentrically braced frames (CBFs). Purlins, supporting the roof cladding and transferring loads from the roof cladding to the rafters, were placed on the rafters with a constant interval. Roof cross braces were arranged in the outer bays to transfer lateral loads to the vertical braces. Full-strength bolted end-plate connections were designed between the apex and eaves. The base connections of the columns and the purlin-rafter connections were designed as pinned. Full-strength gusset plate connections were designed to connect the braces.

Similar to PRC buildings, for each site, four different configurations were considered varying transverse and longitudinal bay widths and story- and crane-bracket heights; denoted as L_x , L_y , H , and H_c , they are provided in Table 2 and shown in Fig. 5a.

The seismic design referred to low-ductility class; seismic actions in horizontal and vertical directions were obtained through MRS analysis from the elastic spectra applying a q factor equal to 4.0. The cross-section designs of structural members for the twenty-four structures resulted in nine different design solutions, as discussed in Scozzese et al. (2018).

The 3D models include geometrical and material non-linearities. Geometrical non-linearities were considered through the large displacements and small strains approach, while material non-linearities were included using distributed plasticity in all structural elements (columns, beams, and braces). Lumped plasticity was used to model the out-of-plane behaviour of the gusset plates at braces' ends, according to the modeling strategy adopted for the braces (Hsiao, Lehman, and Roeder 2013). In addition to the bare-frame models of the considered case studies, models incorporating the non-linear

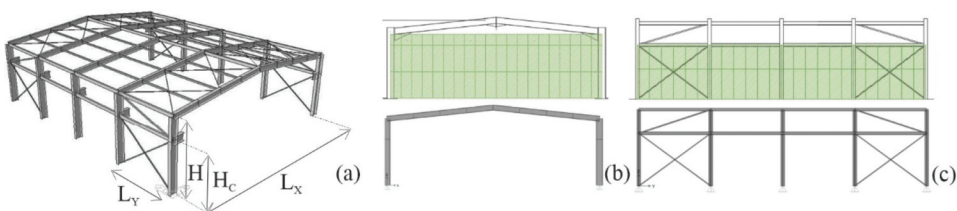


Figure 5. (a) prototype steel frame building; (b) cladding panels distribution in the longitudinal direction; (c) cladding panels distribution in the transverse direction.

Table 2. Geometry parameters for the prototype S buildings.

| Geometry | L_x [m] | L_y [m] | H [m] | H_c [m] |
|----------|-----------|-----------|---------|-----------|
| 1 | 20 | 6 | 6 | 4.5 |
| 2 | 20 | 8 | 6 | 4.5 |
| 3 | 30 | 6 | 9 | 7.5 |
| 4 | 30 | 8 | 9 | 7.5 |

behaviour of the cladding panels were developed. A schematic representation of the cladding panel distribution is given in Fig. 5b, c for the longitudinal and transverse façades, respectively.

The sixty-four structures considered are given in the following code format, TYPOLOGY-LENGTH_IN_X-LENGTH_IN_Y-CLADDING-SITE-SOIL, where the typology is S, X-length can be 20 or 30, Y-length can be 6 or 8, cladding – if present – is indicated as PANELS, site is AQ, NA, or MI, and soil is A or C.

Failure Criteria

In the RINTC project the structural reliability was assessed with respect to the exceedance of two damage states, GC and UPD. The GC criterion was, in general, defined based on an engineering demand parameter (EDP) that is either the roof displacement ratio (RDR) or the maximum inter-story drift ratio (MIDR), the failure limit of which is to a certain level of post-peak strength deterioration; i.e. 50% of the maximum base-shear on the static pushover (SPO) curves of the structures for each main horizontal direction (Fig. 6a). This is the case of the URM, RC, and PRC buildings; however, there are some exceptions or adjustments required for some structural typologies. For the URM buildings, the collapse criteria were defined based on the MIDR of single-wall elements corresponding to a 50% drop of the maximum base-shear from SPO analysis, which was conducted under several load patterns (i.e. uniform or triangular) in both horizontal directions, and the minimum value was defined as the failure threshold. Some adjustments were made in the cases the dynamic deformation capacity was found to be lower than the SPO-based threshold value (possibly because of torsional effects and cyclic degradation). In particular, the threshold was adjusted to the MIDR corresponding to a 35% drop of the maximum base-shear on the static capacity curve of irregular buildings. Particular to PRC buildings, a local collapse condition corresponding to the attainment of the maximum shear strength of the beam-column dowel connections, which is critical for this structural type, was also considered. Given that the S buildings have different load-resisting systems in two horizontal directions, the collapse criteria were defined individually for each of them: 10% RDR was selected for the direction with the MRF system, following the indications by FEMA 350 (2013), whereas the collapse in the CBF system corresponds to the attainment of the maximum strain range, defined as the difference between minimum and maximum strain responses measured at the cross-sections of brace members under seismic excitation. For the latter, the strain range threshold was set according to past studies on local collapse in brace members due to

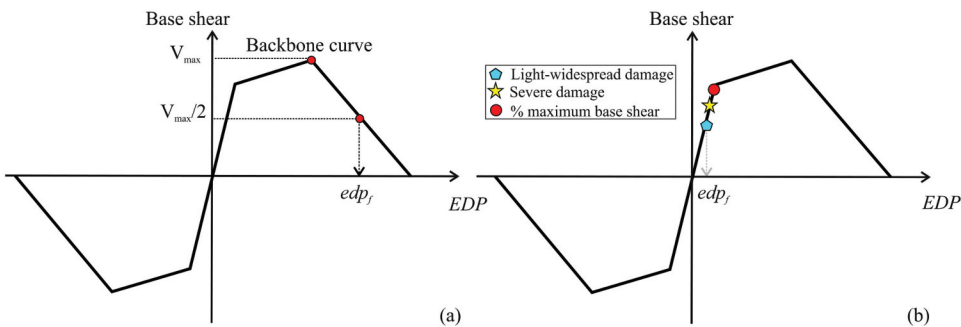


Figure 6. General definition for the GC failure criterion (RC, URM, PRC, and BI) (a) and UPD failure criteria (b). In the latter case, failure is defined as the first occurring among the three conditions defined within the text.

Table 3. Criteria for UPD based on multi-criteria approach for each structural typology.

| Typologies | Multi-criteria approach for UPD | | |
|------------|---|---|--|
| | a | b | c |
| URM | Light-widespread damage in 50% of masonry walls (computed in terms of resisting area) in each direction | At least one of masonry walls reached the drift limit corresponding to a certain level of strength deterioration in the case of the phenomenological non-linear beam or attainment of the toe-crushing condition in the case of the macroelement mechanical model | The attainment of 95% of the maximum base-shear of the structure |
| RC BI | Light-widespread damage in 50% of masonry infills and partitions | At least one of the masonry infills or partitions reached 50% strength drop from its maximum resistance | The first attainment of 95% of the maximum base-shear of the structure |
| PRC | 1% inter-story drift ratio | At least one cladding panel reached the maximum strength of the panel-structure connection, with possible panel overturning | - |
| S | Widespread light damage in 50% of the cladding (sandwich) panels, in each horizontal direction | At least one panel-to-frame connection reached its maximum strength | Having attained 95% of the maximum base-shear of the structure |

low-cycle fatigue (Hsiao, Lehman, and Roeder 2013). The collapse condition for BI reinforced concrete buildings occurs either if the superstructure fails or if the base isolation system fails. The superstructure failure criterion is analogous to the one used for the RC buildings, while the failure of the base isolation was defined based on the device-specific criteria. For HDRBs, three different failure modes were considered; i.e. cavitation, buckling, and shear failure. The global collapse of the isolation system was conventionally deemed to occur when at least half of the devices of the isolation system simultaneously fail due to cavitation, shear, or buckling. For FPSs, the global collapse was deemed to occur when the first device reaches an ultimate displacement in extra-stroke regime, defined considering a limit value of contact pressure and other issues related to sliding material degradation.

UPD (Fig. 6b) occurs at considers the onset of any of the following three conditions:

- light damage in 50% of the main non-structural elements (e.g. infills);
- at least one of the non-structural elements reached a severe damage level;
- attainment of 95% of the maximum base-shear of the structure.

These three conditions specified for each structural typology are summarized in Table 3.

Sites and Hazard

To quantify the risk of failure and to select records for the non-linear dynamic analysis of structures, hazard curves needed to be calculated for the three sites under investigation. They were computed using as the IM the spectral ordinates, $Sa(T)$, closer to the first-mode vibration period of the developed structural models, which is also the IM to develop the fragility curves. This is to warrant some efficiency of the IM, given that the hazard consistent record selection should prevent issues related to sufficiency of the IM (see also Suzuki and Iervolino 2020, for a discussion on these matters). Better efficiency could, in fact, be gathered via advanced IMs (e.g. Bojórquez and Iervolino 2011), but they were avoided so that, when integrating with hazard to obtain the failure rate, the latter could be expressed in terms of a simple IM; moreover, it also facilitates the comparison among fragility curves. Table 4 summarizes the hazard analysis performed and the corresponding IMs.

Hazard curves, expressed in terms of annual exceedance rate, λ_{im} , were computed, via the OpenQuake (Monelli et al. 2012) using the seismic zone source model of Meletti et al. (2008), with the magnitude distribution and rates described in Barani, Spallarossa, and Bazzurro (2009), and the ground motion prediction equation by Ambraseys, Simpson, and Bommer (1996), complemented by that of Akkar and

Table 4. Sites and spectral ordinates where hazard curves were computed.

| Site | Sa(0.15s) | | Sa(0.5s) | | Sa(1s) | | Sa(1.5s) | | Sa(2.0s) | | Sa(3.0s) | |
|---------------|-----------|---|----------|---|--------|---|----------|---|----------|---|----------|---|
| | A | C | A | C | A | C | A | C | A | C | A | C |
| L'Aquila (AQ) | ✓ | ✓ | ✓ | ✓ | ✓ | ✓ | - | ✓ | ✓ | ✓ | - | ✓ |
| Naples (NA) | ✓ | ✓ | ✓ | ✓ | ✓ | ✓ | - | ✓ | ✓ | ✓ | - | ✓ |
| Milan (MI) | ✓ | ✓ | ✓ | ✓ | ✓ | ✓ | - | ✓ | ✓ | ✓ | - | - |

Bommer (2010) for periods beyond 2s. Hazard curves were discretized in ten IM values corresponding to the following return periods in years: $T_R = \{10, 50, 100, 250, 500, 1000, 2500, 5000, 10000, 100000\}$. No IM-values with exceedance return period longer than $T_R = 100000$ years were calculated, to avoid large hazard extrapolations.

The 3D structural models were analysed via MSA, which has the objective of quantifying structural response when IM increases. MSA typically uses different sets of ground motion records at each IM-level so that record selection is hazard-consistent. A procedure based on the conditional spectrum approach (Lin, Haselton, and Baker 2013), which accounts for seismic hazard disaggregation as described in Spillatura et al. (2021), was employed for selecting the ground motion records.

The selected records were extracted mainly from the Italian accelerometric archive (Luzy et al. 2008) and only if no records with similar spectra were available there, records in the NGAwest2 database (Ancheta et al. 2014) were selected instead. The record selection, for each chosen IM, delivered two-hundreds pairs (horizontal components) of records; twenty records for each one of the ten stripes (Fig. 7a shows selection for one stripe). To reduce the computational demand of MSA, the records have been processed to remove the parts of the signal outside the $\{t_{0.05\%}, t_{99.95\%}\}$ range, where $D_{99.90\%} = t_{99.95\%} - t_{0.05\%}$ is the 99.90% significant duration of the record (Dobry, Idriss, and Ng 1978), yet keeping synchronization of horizontal components, which are applied simultaneously.

Dynamic Analysis and Seismic Reliability Evaluation

In the project, the structural models were built in OpenSees (McKenna et al. 2000) except for URM buildings that were analysed using TREMURI (Lagomarsino et al. 2013). The output of the analysis for each building consists of two hundred structural responses (ten stripes of twenty structural responses) obtained from the application of pairs of horizontal records for each of the two main horizontal directions of the 3D model.

For all the models, failure with respect to the performance level of interest (GC and UPD) was checked using the maximum demand-over-capacity ratio in the two directions, herein defined as $edp_{i,j}, i = 1, \dots, 10, j = 1, \dots, 20$. Analysis leads to ten stripes of twenty responses (Fig. 7b).

The rate of earthquakes causing failure of the structure, λ_f , was calculated as:

$$\lambda_f = \int_{IM} P[f|IM = im] \cdot |d\lambda_{im}| \approx \int_0^{im_{T_R, max}} P[f|IM = im] \cdot |d\lambda_{im}| + 10^{-5}, \tag{1}$$

where $P[f|IM = im]$ is the fragility of the structural model, defined as the probability of violating a failure EDP threshold, edp_f , conditional to the values of a ground motion $IM = im$, $|d\lambda_{im}|$ is the absolute value of the derivative of the site-specific hazard curve times $d(im)$, and $im_{T_R, max}$ is the IM value corresponding to $T_R = 100000$ years. Consistent with defining structural response in terms of demand-over-capacity ratio, edp_f is equal to one.

Structural failure was considered to have been reached in cases of *numerical instability*, of the structural analysis, referred to as *collapse* cases, or the attainment of the failure criteria in either of the two horizontal directions. Given that collapse is indicated as C, fragility has been evaluated via an application of the total probability theorem (Shome and Cornell 2000):

$$P[f|IM = im] = P[C|IM = im] + P[EDP \geq edp_f | \bar{C}, IM = im] \cdot \{1 - P[C|IM = im]\}, \tag{2}$$

where $P[\text{EDP} \geq \text{edp}_f | \bar{C}, \text{IM} = im]$ and $P[C | \text{IM} = im]$ are, given IM, the probability of failure given non-collapse and collapse, respectively.

Because site-specific hazard curves in the RINTC project were evaluated for ten return periods T_R with an upper bound equal to 100000 years, it has been conservatively assumed that ground-motions having IM larger than $im_{T_R, \max}$ certainly cause failure, as shown in the last equality of Eq. (1), where 10^{-5} is added to the integral to account for the truncation of the hazard curve at $\lambda_{im} = 10^{-5}$ (this addition can dominate λ_f at the low-hazard sites). The discretization of the structural analysis at the ten IM levels and the use of twenty pairs of ground motions at each IM stripe yielded the following approximation in computing Eqs. (1) and (2):

$$100000 \quad (3)$$

Assuming that the distribution of the probability of failure given non-collapse is lognormal (Romão, Delgado, and Costa 2014; Shome and Cornell 2000) in the equation: $\Phi(\cdot)$ is the cumulative Gaussian distribution function, m_{C, im_i} is the number of collapse cases at the im_i stripe and $\left\{ \mu_{\ln(\text{EDP}) | \bar{C}, im_i}, \sigma_{\ln(\text{EDP}) | \bar{C}, im_i} \right\}$ can be interpreted as the mean and the standard deviation of the logarithms of EDP at the im_i stripe; also $P[C | \text{IM} = im_i] = m_{C, im_i} / 20$.

The main result emerged from the project was that the seismic reliability increases when the design seismic hazard decreases. This happens even though the design seismic actions have the same (assigned) probability of being exceeded during a time interval at each site. Further research has shown that two different issues could possibly explain this result: (i) the first one is related to the requirements that the code imposes regardless of the design seismic actions, for example, the minimum reinforcement requirements and gravity load design, which tend to dominate in the low hazard sites providing larger seismic reliability with respect to structures located in sites where the seismic actions dominate the design (Baltzopoulos, Grella, and Iervolino 2021); (ii) the expected shaking intensity given the exceedance of the design ground motion, which is disproportionally larger for high-hazard sites with respect to mid-hazard and low-hazard sites (Cito and Iervolino 2020).

Lognormal Fragility Fitting

In the framework of PBEE, two predominant approaches exist to estimate fragility functions analytically, namely IM-based and EDP-based according to the terminology of Vamvatsikos and Cornell (2005), the difference lying in the characterization of demand and capacity terms. In the first case, incremental dynamic analysis (Vamvatsikos and Cornell 2002) is typically performed to obtain a sample of a random variable, that is, the IM causing structural failure. In the EDP-based approach, the fragility function is evaluated as the probability that the random variable, defined by the EDP conditional to any IM level, is larger than edp_f . Consistent with the described project's approach, herein the fitting approach was the EDP-based. The IM to express the fragility is the one to perform MSA for the considered structural model (see the Appendix).

If the lognormal probability model is chosen, fragility can be expressed as:

$$P[f | \text{IM} = im] \triangleq \Phi \left[\frac{\ln(im) - \eta}{\beta} \right], \quad (4)$$

where $\{\eta, \beta\}$ can be interpreted as the mean and standard deviation of the logarithms of the IM causing failure.

The maximum likelihood (ML) fitting method seeks the parameters $\{\eta, \beta\}$ such that the resulting distribution has the highest likelihood of having generated the observed data (Baker 2015). In MSA, at each of the n stripes (ten in the RINTC project), a total number, m , of structural analysis is conducted (twenty in the RINTC project) so that, vectors of the kind

$edp_i = \{edp_{i,1}, edp_{i,2}, \dots, edp_{i,m}\}, i = 1, 2, \dots, n$, are finally available. Each of these vectors can be partitioned in two: one with failure and collapse cases, of size m_{f,im_i} , and one of non-failure and non-collapse cases, of size $(m - m_{f,im_i})$. Then the ML can be written as:

$$\{\eta, \beta\} = \underset{\eta, \beta}{\operatorname{argmax}} \left[\sum_{i=1}^n \left(\ln \binom{m}{m_{f,im_i}} + m_{f,im_i} \cdot \ln \left\{ \Phi \left[\frac{\ln(im_i) - \eta}{\beta} \right] \right\} + (m - m_{f,im_i}) \cdot \ln \left\{ 1 - \Phi \left[\frac{\ln(im_i) - \eta}{\beta} \right] \right\} \right) \right]. \quad (5)$$

ML was considered the preferred fitting method herein as it is a consolidated statistics approach to estimate the fragility parameters; however, it requires a certain number of failure cases be observed across the IM stripes. When the structural vulnerability is low compared to the seismic hazard at the site, results from MSA may provide only a few failures, if any, at each IM level. Therefore, alternative approaches may be needed in these situations, and two of them were considered in this study.

The first one, GPP, is based on a Gaussian probability plot (e.g. Benjamin and Cornell 1970). Given that n lumped fragility values, $P[f|IM = im_i], i = \{1, 2, \dots, n\}$, evaluated as per the second Eq. (3) are available for each of the stripes, based on the non-collapse vectors of stripe responses, $\{edp_{i,1}, edp_{i,2}, \dots, edp_{i,m_{C,im_i}}\}, i = 1, 2, \dots, n$, this approach consist of an ordinary least square regression of $\{\ln(im_i), z_i\}$ data, where $z_i = \Phi^{-1}\{P[f|IM = im_i]\}$, that is:

$$\{\eta, \beta\} = \underset{\eta, \beta}{\operatorname{argmin}} \left[\sum_{i=1}^n \left(\Phi^{-1} \left\{ \frac{m_{C,im_i}}{m} + \left[1 - \Phi \left(\frac{\ln(edp_f) - \mu_{\ln(EDP)|\bar{C},im_i}}{\sigma_{\ln(EDP)|\bar{C},im_i}} \right) \right] \cdot \left(1 - \frac{m_{C,im_i}}{m} \right) \right\} - \frac{\ln(im_i)}{\beta} + \frac{\eta}{\beta} \right)^2 \right]. \quad (6)$$

A second alternative approach, based on least square fit (LSF), computes the fragility minimizing the sum of squared errors between the lumped fragility values and probabilities of collapse predicted by the lognormal fragility function, which yields the curve’s parameters as:

$$\{\eta, \beta\} = \underset{\eta, \beta}{\operatorname{argmin}} \left(\sum_{i=1}^n \left\{ \frac{m_{C,im_i}}{m} + \left[1 - \Phi \left(\frac{\ln(edp_f) - \mu_{\ln(EDP)|\bar{C},im_i}}{\sigma_{\ln(EDP)|\bar{C},im_i}} \right) \right] \cdot \left(1 - \frac{m_{C,im_i}}{m} \right) - \Phi \left(\frac{\ln(im_i) - \eta}{\beta} \right) \right\}^2 \right). \quad (7)$$

GPP and LSF are considered heuristic and somewhat equivalent for the purposes of this work. In fact, all the three methods were applied to the data, and one of the two, between LSF and GPP, was chosen based on qualitative evaluation of the fitting in those cases where ML was considered unsatisfactory.

Estimation Uncertainty

Because of record-to-record variability, the parameters $\{\eta, \beta\}$ are expected to change when the sample of records changes. Therefore, the fragility fitting equations shown above only provide an estimation of the parameters that should be indicated as $\{\hat{\eta}, \hat{\beta}\}$, and the distribution of which quantifies the uncertainty in fragility assessment (Baraschino, Baltzopoulos, and Iervolino 2020; Iervolino 2017; Skoulidou and Romão 2019). For the sake of simplicity, $\{\eta, \beta\}$ symbols are hereafter used, instead of the more appropriate $\{\hat{\eta}, \hat{\beta}\}$. Depending on the procedure used for fragility fitting, the distribution of $\{\eta, \beta\}$ are quantified with a specific procedure based on resampling. In particular, for ML, given $\{\eta, \beta\}$ obtained from original data, at each IM stripe a new number of failures (and non-failures consequently) is extracted from a binomial distribution with parameter $p_i = \Phi[(\ln(im_i) - \eta)/\beta]$, then Eq. (5) is applied again to obtain a new $\{\eta, \beta\}$. In the case of GPP and LSF the vectors $\{edp_{i,1}, edp_{i,2}, \dots, edp_{i,m}\}, i = 1, 2, \dots, n$, vectors are resampled with replacement; then Eq. (3) and subsequently Eq. (6) or Eq. (7) are applied again. These procedures can be repeated an arbitrary number of times to obtain a distribution of the parameters for the case under examination. Details on the fragility fitting procedures used in this paper and the related estimation uncertainty are described in detail in Iervolino (2022).

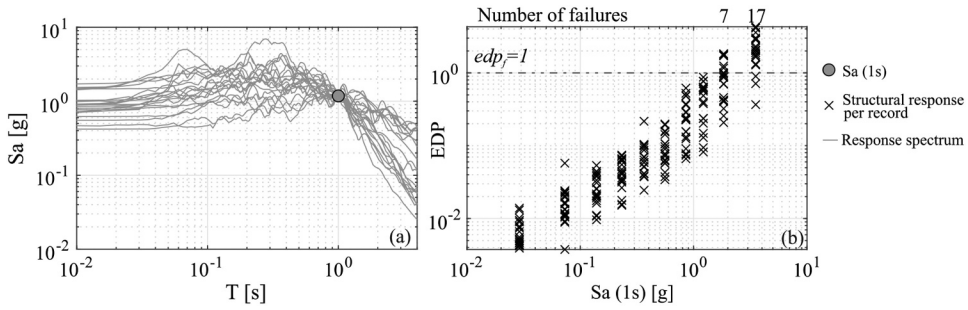


Figure 7. (a) Example of hazard-consistent record-selection for MSA; (b) example of MSA results when the EDP is the demand-to-capacity ratio.

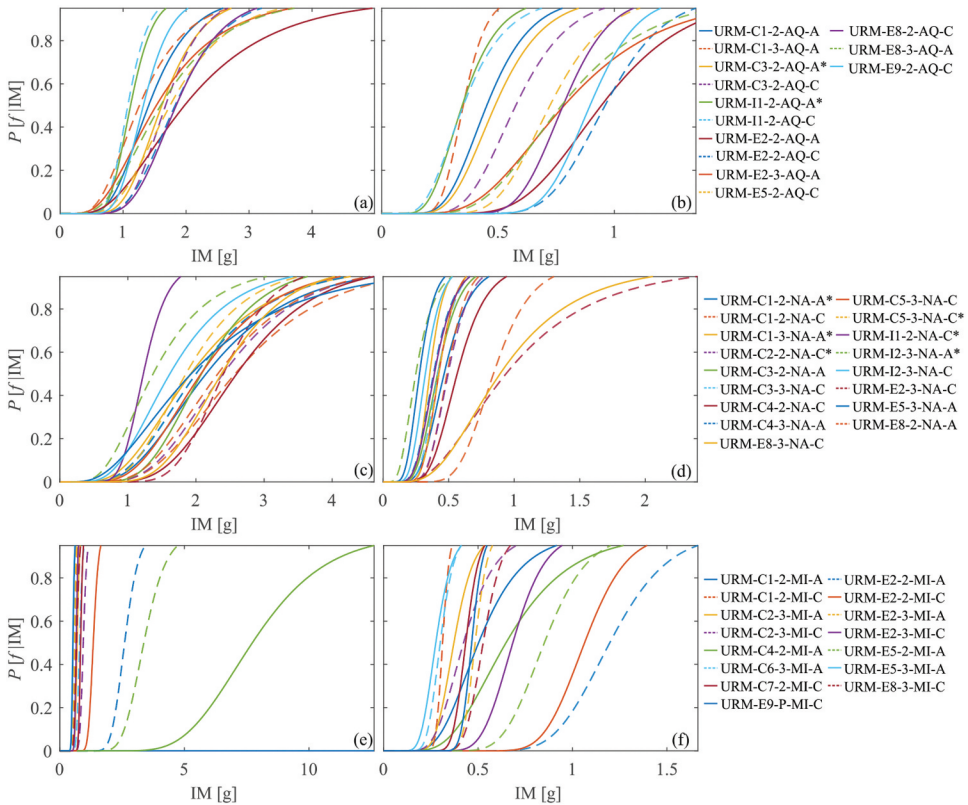


Figure 8. Fragility curves for URM buildings. Figures show curves for L'Aquila (a,b), Naples (c,d) and Milan (e,f) at GC and UPD, respectively.

Results and Discussion

Fragility Curves

The fragility fitting and uncertainty in estimation procedures introduced above are implemented in R2R-EU software (Baraschino, Baltzopoulos, and Iervolino 2020), which was used to get the results presented in this section. One of the fragility derivation methods described above was chosen for each case, on the basis of qualitative evaluation of how the curve fitted the lumped fragility values (the

results of the three procedures for each model cannot be given here for the sake of brevity). Figures representing the lognormal fragilities are shown in Figs. 8–12, while lognormal parameters for each structure are listed in the Appendix. In all the figures, abscissa axis is limited to the IM value corresponding to the 95th percentile of the fragility curve with maximum η (but lower than 3 to keep figures readable) among those belonging to the same structural typology, design site, and for the same failure criteria. These figures are given to provide the reader with a graphical representation of the curves the parameters of which are given in the Appendix.

Fragility curves generally show a large parameters' variability, even for structures belonging to the same structural typology at the same site. This partly depends on the fact that the curves are poorly constrained by non-linear dynamic analysis results (in turn, a question may arise about the curves' usability in seismic risk evaluation, which is discussed in the following section). More specifically, defining the lumped fragility values as $P[f|IM = im_i] = m_{f,im_i}/m$, (i.e. the empirical percentiles according to the terminology of Baraschino, Baltzopoulos, and Iervolino 2020), past research (i.e. Baker 2015) has shown that some issue may occur when the IM levels at which the lumped fragility is evaluated, discretize in some manner the IM domain. Intuitively, the curve is best constrained when the IM discretization at which dynamic analysis is performed gives a large and densely populated range of $P[f|IM = im_i]$ from 0% to 100%. The fixed IM levels adopted in the RINTC project lead to a series of situations that can be summarized by those sketched in Fig. 13, where the lumped fragility values are plotted against the result of the fitting procedure (black solid line) for four buildings, chosen as an example.

The level of constraint to the fragility can be quantified by the estimation uncertainty of the parameters. To illustrate this issue, the fitting procedures have been applied to four among the

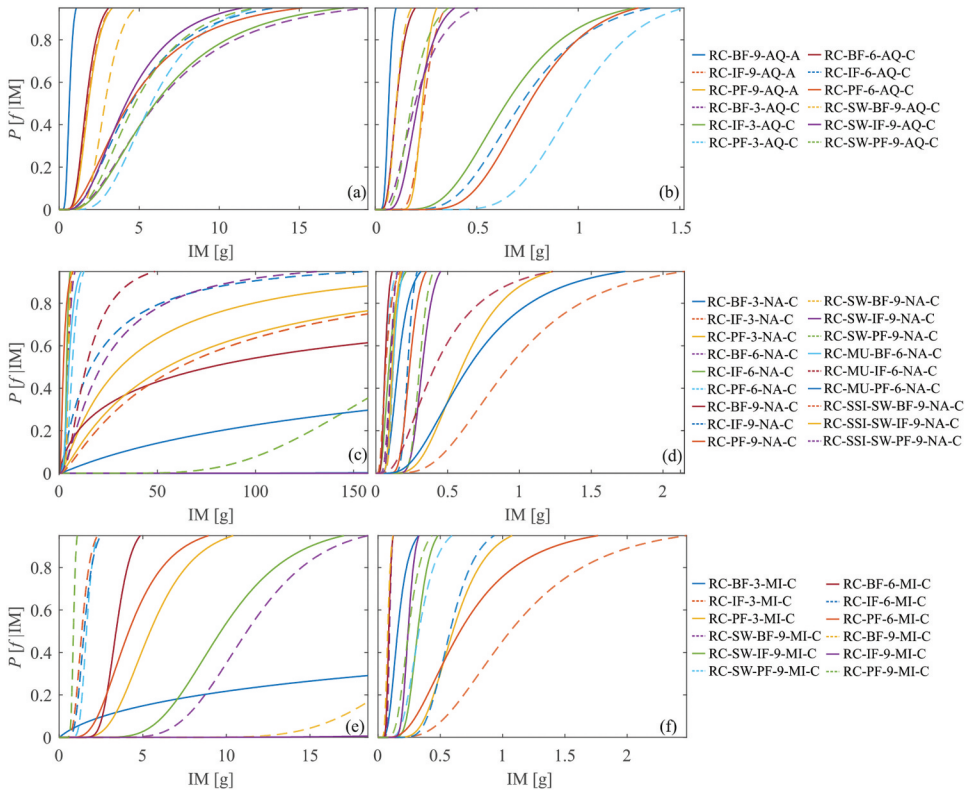


Figure 9. Fragility curves for RC buildings. Figures show curves for L'Aquila (a,b), Naples (c,d) and Milan (e,f) at GC (left) and UPD (right) respectively.

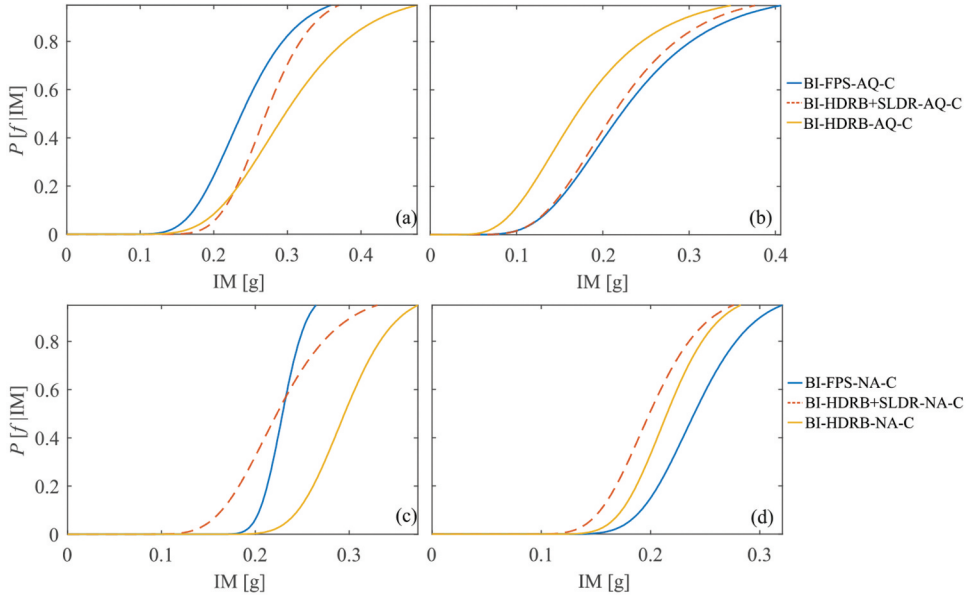


Figure 10. Fragility curves for BI buildings. Figures show curves for L'Aquila (a,b) and Naples (c,d) at GC (left) and UPD (right), respectively.

investigated case studies that are the BI building identified as BI-FPS-AQ-C, the S building S-LX30-LY8-AQ-A, the URM building URM-C1-2-NA-A, and the RC building RC-BF-3-MI-C. Fragilities have been assessed (at GC) by using ML, for the first, third, and fourth buildings, while LSF for the second one. Subsequently the distribution of the fragility parameters has been quantified for each case by means of the resampling-based procedures repeated $k = 500$ times. The fragility curves are given in Fig. 13, where the grey thin lines represent the 500 curves from resampling.

The root mean square error of the sample standard deviation of the fragility curves, given that β_i^* is the lognormal standard deviation from i -th simulation, has been evaluated as:

$$RMSE = \sqrt{\frac{\sum_{i=1}^k \left(\frac{\beta_i^* - \beta}{\beta}\right)^2}{k}}, \quad i = 1, 2, \dots, 500. \quad (8)$$

Defining the maximum values of the lumped fragility (from now on LFM) as: $LFM = \max(P[f|IM = im_i])$, $i = 1, 2, \dots, 10$, where im_{10} is the intensity corresponding to an exceedance return period of 10^5 years at the site of interest, it allows to identify different situations/issues. (Note that, for the first, third and fourth cases $P[f|IM = im_i] = m_{f,im_i}/m$, while for the second one it is assessed according to the second Eq. (3).)

- $LFM \approx 1$ means that in one of the ten stripes at least, all the records applied to the structure lead to failure and/or collapse. Capacity of the fragility fitting is considered well constrained. As a reference, RMSE is equal to 0.18 in this case (Fig. 13a).
- $LFM \approx 0.60$ means that the data from dynamic analysis are available up to IM levels slightly above the median. Fragility fitting continues to well represent the trend of the empirical data, but the estimation uncertainty increases with RMSE equal to 0.21 (Fig. 13b).
- $LFM \approx 0.30$ means that empirical data are available up to IM level lower than the median. Curve fitting is somewhat getting worse and estimation uncertainty greatly increases with a RMSE equal to 0.32 (Fig. 13c).

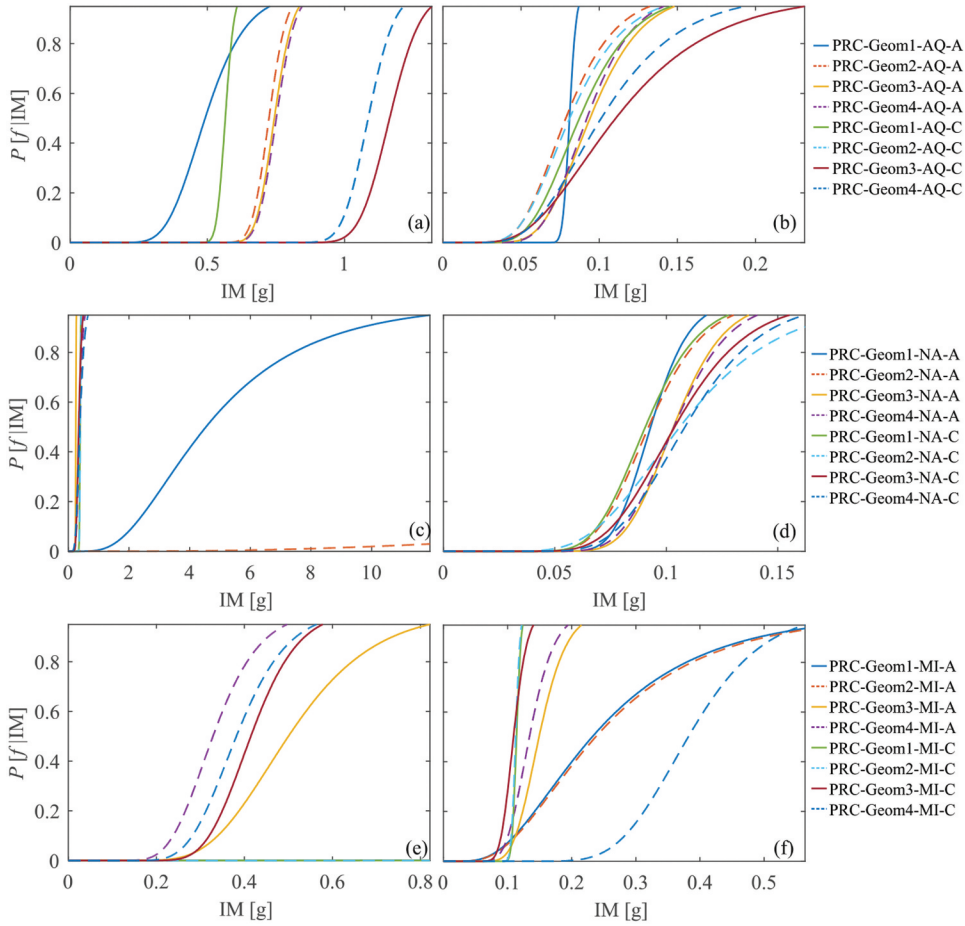


Figure 11. Fragility curves for PRC buildings. Figures show curves for L’Aquila (a,b), Naples (c,d) and Milan (e,f) at GC and UPD, respectively.

- LFM = 0.05 means that no failures and/or collapses occur in nine over ten stripes and only one failure occurs in the remaining stripe. Fragility curve is extrapolated for $P[f|IM = im]$ values greater than 0.05, with RMSE equal to 1.30 (Fig. 13d).

Summarizing what observed, when LFM decreases, the heterogeneity of the parametric resampling around the black solid line tend to increase. For this reason, RMSE increases when LFM decreases, showing that, as expected, the estimation of the lognormal parameters gets worse when LFM is not high enough to warrant that the fitted curve is well constrained by lumped fragility values. Analogous considerations could be made even if the GPP method is used to estimate fragility parameters. LFM, for all the structures, is listed in the Appendix along with the fragility fitting results.

As it could be expected, the fragility curves for structures designed in the low-seismicity area are most likely to exhibit results affected by high estimation uncertainty because of the comparatively small number of failure cases for each IM-stripe. Conversely, this issue more rarely occurs for the structures designed on high-seismicity area (see also Suzuki and Iervolino 2021). These fitting issues could be addressed by using a larger number of records for each stripe and/or increasing the number of return periods at which the IM stripes are evaluated, but this is not the focus of the study herein presented, which is based on the results of the RINTC project.

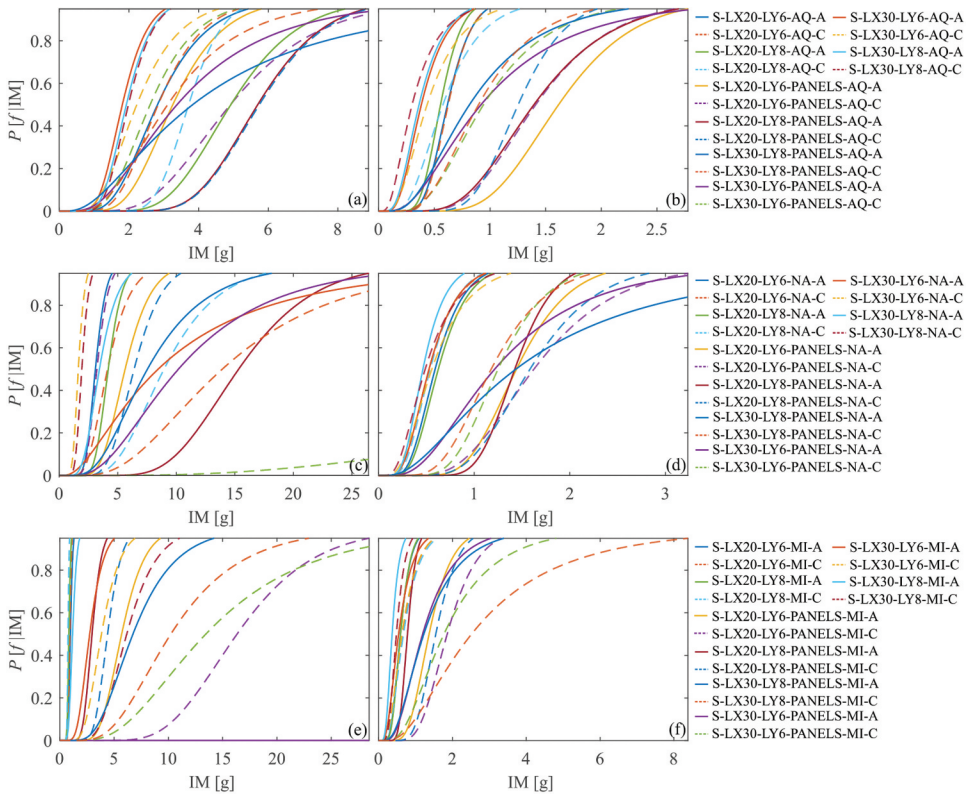


Figure 12. Fragility curves for S buildings. Figures show curves for L'Aquila (a,b), Naples (c,d) and Milan (e,f) at GC and UPD, respectively.

In all the figures, where fragility curves show large parameters variability, in particular large values of the β parameter, the case is similar to those described in Fig. 13c, d. The lower is LFM, more fragility curves are unsuitable to well represent structural behaviour, being results with $LFM < 0.50$ to be handled carefully. Some detailed observation can be worth discussing.

- At GC, fragility curves for the structures designed in the low-hazard site show relatively large estimation uncertainty of parameters, because of the small number of structural failures. This happens for all the structural typology (BI buildings have not been designed in Milan). Among the others, this occurs for the three-story, BF, RC building sites in Milan on soil C (RC-BF-3-MI-C), the S building in Milan on soil A identified as S-LX30-LY6-PANELS-MI-A, the PRC building having ID PRC-Geom4-MI-C, and the URM building URM-C1-2-MI-A. In these cases, fragility fitting issues are the same as those shown in Fig. 13c, d.
- At GC, fragility curves for the structures designed in the mid-hazard site show similar fitting issues except for most of URM buildings and BI buildings. This happens, that is, for the RC building RC-SW-PF-9-NA-C, for the S building S-LX30-LY6-PANELS-NA-C and for the PRC building PRC-Geom2-NA-A. The results show that all the possible cases described in Fig. 13 are faced. All the RC buildings, except the case RC-9-PF-NA-C having $LFM = 0.15$, and S buildings have $LFM \leq 0.05$, falling into the case described in Fig. 13d. All the BI buildings have $LFM = 1$, reflecting the situation described in Fig. 13a. URM buildings spread within a range from $LFM = 0.27$ and $LFM = 1$.
- At GC, fragility curves for structures designed in the high-hazard site seem to provide more constrained results for all the typologies except for PRC buildings, where five over eight cases

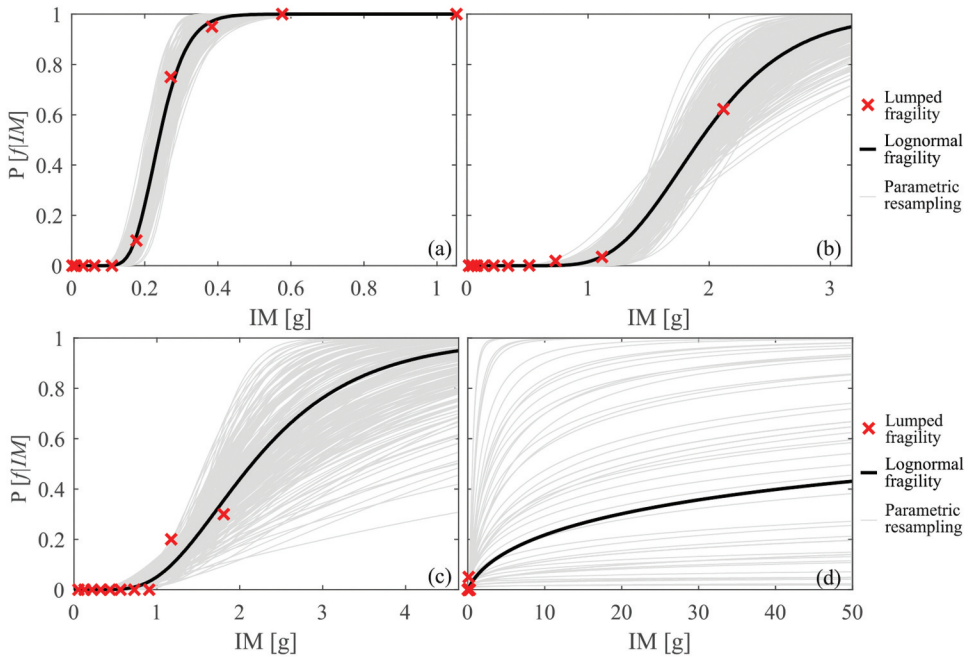


Figure 13. Fragility curves and parametric resampling for four different buildings exhibiting different LFM: 1 (a), 0.60 (b), 0.30 (c) and 0.05 (d).

show $LFM < 0.50$. Most of the buildings fall into the situation depicted in Fig. 13a and b, that is, RC building RC-PF-6-AQ-C, PRC-building PRC-Geom1-AQ-A, URM building URM-I1-2-AQ-C, S building S-LX30-LY8-AQ-C, and BI building BI-FPS-AQ-C.

- Such considerations can be extended to the results at UPD, with a global reduction of the estimation uncertainty due to the increase of failure cases which leads to the increase of LFM.

The estimation uncertainty produced by the lognormal distribution fitting procedure of the empirical data propagate to the failure rate (see the next section) in a way that is also affected by the shape of the hazard curves, which tend to give more emphasis to the values located toward the left tail of the fragility function. It should be finally noted that in nine, over one-hundred-sixty-nine structures (three BI, four S and two URM), the GC and UPD curves for the same building intersect, which should not happen. In most cases (six) it is due to the small number of failures that leads to not-well constrained curves. For the other three cases it is due to the shape of the lognormal curve that is flatter for the UPD than GC.

Curves' Validation and Usability

To validate the obtained fragility curves with respect to the failure rates computed in the RINTC project, the rates were also computed using the fitted curves, that is, via the following equation:

$$\lambda_f(\eta, \beta) = \int_{IM} \Phi \left[\frac{\log(im) - \eta}{\beta} \right] \cdot |d\lambda_{im}| \tag{9}$$

To integrate hazard curves in an IM range larger than those considered in the RINTC project (i.e. return period up to 100,000 years) PSHA was performed again via REASSESS software (Chioccarelli et al. 2019) for the sites in terms the spectral accelerations at the periods at which the curves have been developed (0.15s, 0.50s, 1.0s, 1.5s, 2.0s, and 3.0s) on soil conditions A and C. The seismic zone source

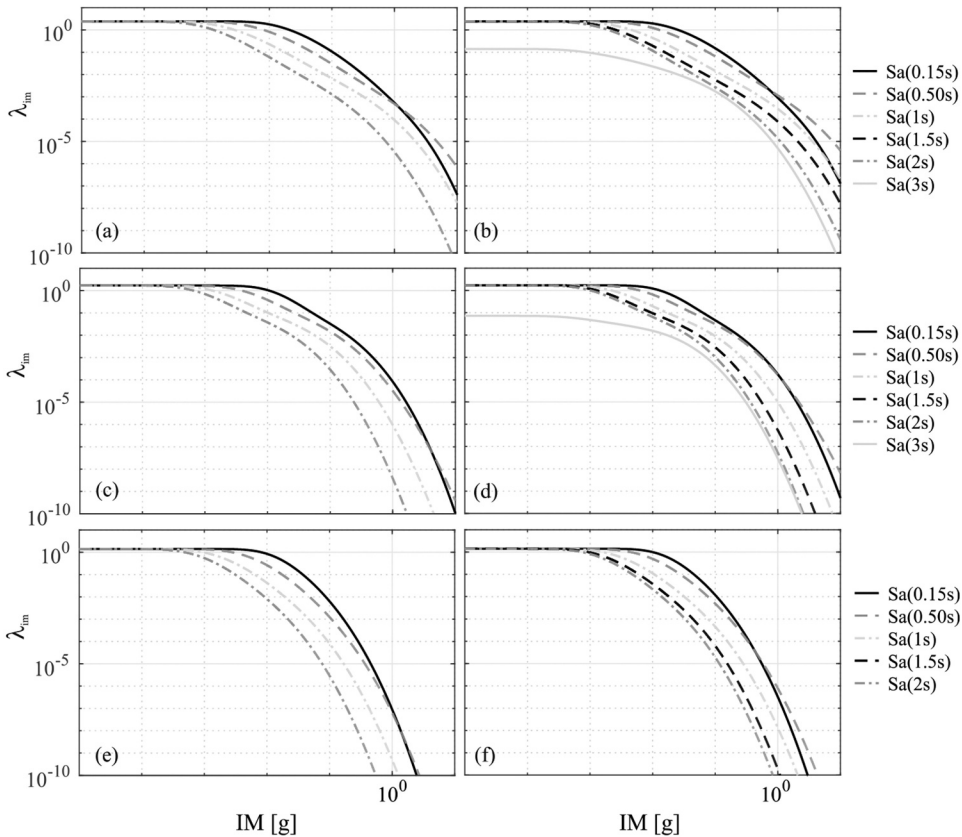


Figure 14. Hazard curves for soil condition A and C respectively for L'Aquila (a,b), Naples (c,d), and Milan (e,f).

model, magnitude distribution, and rates and ground motion prediction equations are the same described in the Sites and hazard section and the resulting curves are shown in Fig. 14.

Combining the fragility curves shown in Figs. 8–12 with the relevant hazard curves among those shown in Fig. 14, Eq. (9) provides the failure rates shown in Fig. 15a, c for GC and UPD and listed in the Appendix.

Apparently, looking at Fig. 15, where colors identify different buildings within the same structural typology, there is a general coherency with the results of the RINTC project (Fig. 15b, d) and the rates computed via the fitted fragility. Differences among the procedures occur more evidently when only a few, if any at all, failure cases from dynamic analysis are observed up to the largest IM stripes (e.g. for structures designed at low-to-mid hazard); this implies that the estimates of the lognormal fragility parameters could be relatively uncertain. As an example, evaluation of the rate of failure at GC for a RC structure sited in Milan, identified with the ID RC-BF-3-MI-C (grey circle in Fig. 15a, b), is deepened: it is equal to $1.19 \cdot 10^{-4}$ when lognormal fragility is considered while it is equal to 10^{-5} using RINTC procedure; i.e. Eq. (3). Structural responses do not exhibit any failure cases and only one collapse case at eighth stripe with a probability of failure $P[f|IM = im]$ equal to zero for each IM value except for $IM = 0.123g$ where it is equal to 0.05. Fig. 16a shows lumped fragility values $P[f|IM = im]$, lognormal fragility, and hazard curve (right vertical axis). The difference of one order of magnitude of the failure rate between two procedures is caused by the lognormal fragility fit which gives values of probability of failure different from zero at low levels of IM where the hazard magnitude is more relevant. Fig. 16b shows the impact of the specific IM-level contribution to the failure rate.¹

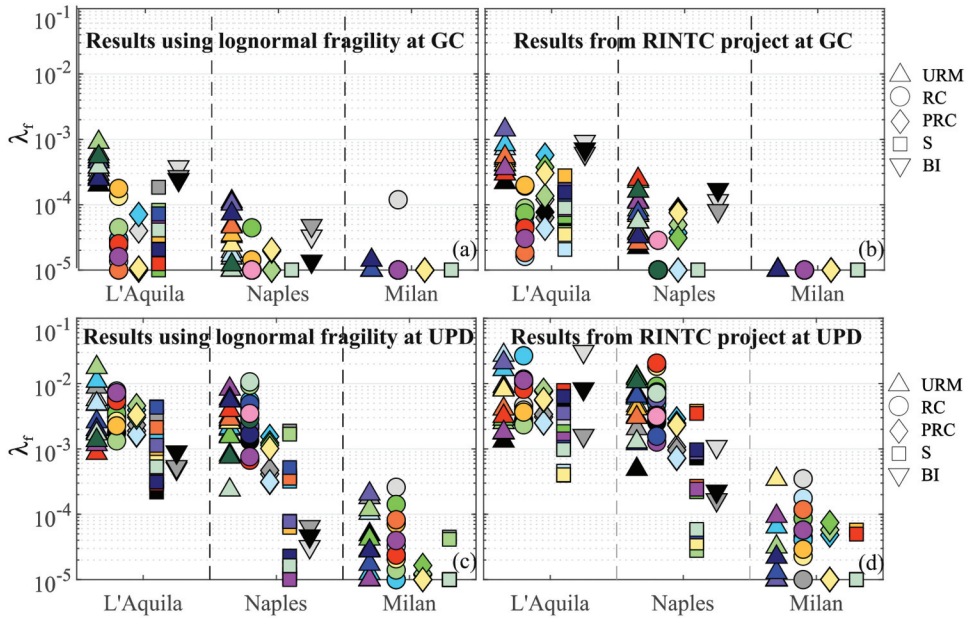


Figure 15. Failure rates evaluated by means of lognormal fragility curves for GC (a) and UPD (c) and using the procedure implemented in RINTC project for GC (b) and UPD (d). Colors represent different buildings in each typology.

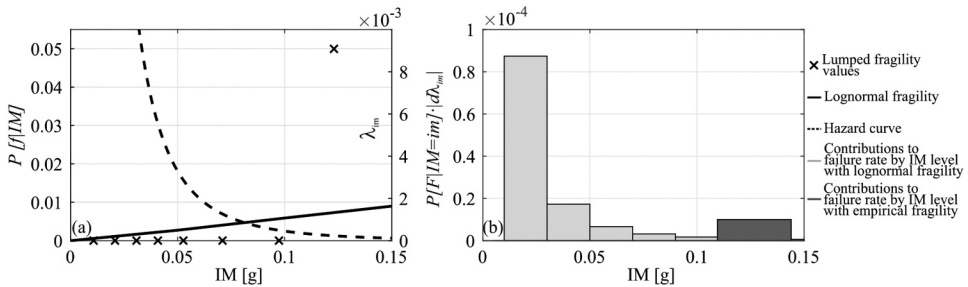


Figure 16. Lumped fragility, lognormal fragility and hazard curve for the structure identified by the ID RC-MI-C-3-BF (a); contributions to failure rate by IM level (b).

With the purpose of a quantification of how much the estimation uncertainty involved in the fragility fitting procedure impacts on the seismic rate evaluation and to investigate about curves' usability, parametric resampling, evaluated in the previous section for four structures, was calculated for all the structures under investigation.²

Given the couple of parameters defining lognormal fragility from the *i*-th simulation, indicated as $\{\eta_i^*, \beta_i^*\}$, the corresponding rate, $\lambda_{f,i}^*(\eta_i^*, \beta_i^*)$, can be evaluated via Eq. (9) to finally obtain a distribution of the failure rates varying $i = 1, 2, \dots$. The coefficient of variation (a sort of, in fact) of such a failure rate distribution can be evaluated as:

$$CoV[\lambda_f] = \frac{STD[\lambda_f]}{E[\lambda_f]} = \frac{\sqrt{\frac{1}{k-1} \cdot \sum_{i=1}^k (\lambda_{f,i}^* - E[\lambda_f])^2}}{\frac{1}{k} \cdot \sum_{i=1}^k \lambda_{f,i}^*}, i = 1, 2, \dots, k. \tag{10}$$

where $STD[\lambda_f]$ and $E[\lambda_f]$ are the standard deviation and the mean of the estimator of the failure rate and $k = 500$. In Fig. 17 $CoV[\lambda_f]$ has been related to the LFM for all the structures involved in RINTC project, grouped by typology and site (red, cyan and green markers identify buildings located in L'Aquila, Naples and Milan respectively).

The analysis of the results for GC (Fig. 17a) suggests the following.

- When LFM is lower than 20%, $CoV[\lambda_f]$ reaches high levels, sometimes larger than one. This happens for all the buildings, belonging to all the typologies, designed in Milan where the minimum $CoV[\lambda_f]$ is about equal to 0.8 and the LFM is lower than 5%. Such a conclusion is the same for buildings designed in Naples (60% out of the total for this site,) while for L'Aquila the number of buildings in this range is on two (out of fifty-two).
- When LFM lies within the range of 20% and 50%, which includes 22% of the buildings designed in Naples and 23% of the buildings designed in L'Aquila, $CoV[\lambda_f]$ decreases with a high intra-site variability from 0.32 and 1.60 for the mid-hazard site 0.24 and 1.21 for the high-hazard site.
- When LFM is larger than 50%, $CoV[\lambda_f]$ drops to values under 20%. In this range lies the 18% of the buildings designed in Naples and more than 75% of the buildings designed in L'Aquila.

For GC, results referring to buildings designed in the low-hazard site (Milan) suggest that fragility fitting provides particularly uncertain parameters estimates; therefore, these curves must be used with caution, at least considering estimation uncertainty in the risk analysis. Results for code-conforming structures in high-hazard site (L'Aquila) suggest that fragility fitting is well constrained, therefore they can be of reference for other similar structures. For the mid-hazard site (Naples) the trend of results is ambiguous, it is then suggested to consider estimation uncertainty in risk analysis carried out employing these curves.

The analysis of results for UPD (Fig. 17b) suggests the following.

- About 90% of the S structures (14 over 16) in Milan have LFM lower than 7% (minimum $CoV[\lambda_f] \approx 0.80$). The remaining two structures show LFM about 35% and $CoV[\lambda_f] \approx 0.36$.
- About 75% (11 over 15) of the URM structures in Milan have LFM lower than 15% and show minimum $CoV[\lambda_f]$ equal to 0.50. 2 out of 15 structures do not exceed 60% LFM while only one structure shows $CoV[\lambda_f]$ lower than 0.20.
- Any PRC structure shows $CoV[\lambda_f]$ larger than 0.50, independently of the LFM value.
- 50% (6 over 12) of the RC structures in Milan show LFM greater than 60% with $CoV[\lambda_f]$ ranging from 0.16 and 0.35; for 5 over 6 structures remaining, LFM varies from 0.25 and 0.40 with $CoV[\lambda_f]$ within a range from 0.24 and 0.6; only one structure shows a $CoV[\lambda_f] \approx 2$ (LFM lower than 5%).
- All the BI structures in mid- and high-hazard sites show $CoV[\lambda_f]$ lower than 0.20.

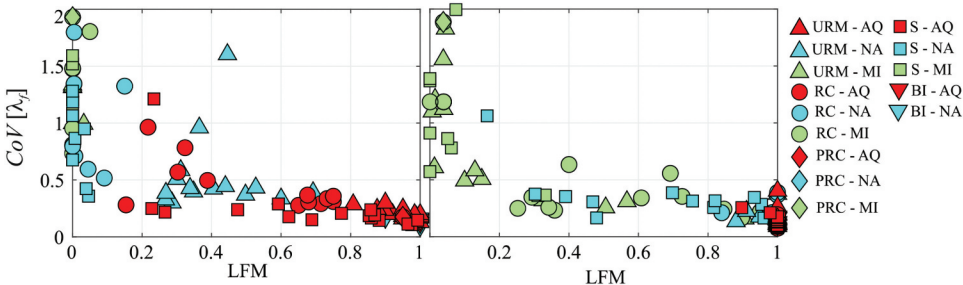


Figure 17. Coefficient of variation of failure rate versus LFM for each structure designed within RINTC project for GC(a) and UPD(b).

At UPD fragility curves for structures designed in Milan may poorly explain the seismic vulnerability for all the typologies except, apparently, for RC buildings. For mid- and high-hazard sites conclusions are essentially equivalent: $CoV[\lambda_f]$ ranges from 7% to 40% for all the structures belonging to all the investigated typologies except for two (over sixteen) steel structures exhibiting $CoV[\lambda_f]$ larger than one. Values of $CoV[\lambda_f]$ at GC and UPD are listed in the [Appendix](#).

Conclusions

In the presented study parametric fragility curves for global collapse and usability preventing damage, for the buildings analysed within RINTC project, were derived. The structures, belonging to a variety of structural types and configurations, were designed for damage and life safety, according to the Italian code, for two soil conditions at three sites characterized by seismic hazard ranging from low-to-high in the country. Starting with results of the multi-stripe analysis performed within the project, up to IM levels corresponding to 100000 years exceedance return period at the construction site, EDP-based lognormal fragility was assessed, for all the code-designed structures. The fitting methods include quantification of estimation uncertainty that can be carried over the evaluation of the seismic structural reliability expressed in terms of failure rates.

The results show significant heterogeneity of fragility parameters within each typology and among typologies. This mainly derives from the number of failures observed in the structural dynamic analysis in the range of IMs at which they are performed. This has been investigated looking at the estimation uncertainty in the fragility parameters and the consequent variability of the failure rates when these curves are integrated with the site's hazard. The main resulting remarks are listed here.

- For GC, fitting for all the typologies of structures designed at low-site hazard provides fragilities deemed weakly constrained, in general. This could be motivated by the requirements that the Italian code imposes regardless of the design seismic actions leading to structures which under strong seismic actions do not exhibit any (or exhibit very few) failure cases. To have structural analysis performed at IM levels, so as to obtain lumped fragility values densely covering the (0,1) interval could improve fragility fitting and reduce the related issues. Conversely, results for structures designed at the high-hazard site suggest that estimated fragility parameters better represent structural behaviour of all the buildings belonging to all the typologies. For the mid-hazard site, the trend in the results is not particularly clear.
- At UPD, S, URM, and PRC structures designed at the low-hazard site have fragility parameters which are also relatively poorly constrained. Only for RC structures designed at Milan, fragilities give results, which may indicate the possibility to use the curves with some trust.
- At UPD, for mid- and high-hazard sites conclusions are essentially equivalent for almost all the buildings belonging to all the typologies: parameters of fragility functions seem to be somewhat explanatory of structural seismic vulnerability.

With these considerations in mind, these curves are made available for further risk assessment studies involving code-conforming buildings.

Notes

1. Differences among failure rates of BI buildings designed in L'Aquila are not strictly related to fragility fitting, yet by the hazard curves used for the validation, which are not exactly those of the RINTC original study.
2. For all the structures, fragility fitting method to evaluate $\{\eta^*, \beta^*\}$, shown in [Tables 5–9](#), is the same as that used to get $\{\eta, \beta\}$.

Acknowledgments

The study presented in this article was developed within the activities of the 2019-2021 ReLUIIS-DPC and EUCENTRE-DPC research programs. However, the opinions and conclusions herein discussed may not be shared by the funding entity. Authors also acknowledge the contribution to this study of the broader RINTC workgroup.

Authors' Contribution Statement

I. Iervolino developed the procedures adopted in the paper and drafted the manuscript; R. Baraschino coded the procedures and drafted the manuscript; A. Belleri and G. Magliulo produced the results for PRC buildings and reviewed the manuscript; D. Cardone and L.R.S. Viggiani produced the results for BI buildings and reviewed the manuscript; G. Della Corte and A. Zona produced the results for S. buildings and reviewed the manuscript; P. Franchin and A. Marchi produced the results for RC buildings and reviewed the manuscript; S. Lagomarsino and A. Penna produced the results for URM buildings and reviewed the manuscript.













Disclosure Statement

No potential conflict of interest was reported by the author(s).

Funding

The work was supported by the Consorzio della Rete dei Laboratori Universitari di Ingegneria Sismica (ReLUIIS) [ReLUIIS-DPC 2019-2021 research program].

ORCID

Iunio Iervolino  <http://orcid.org/0000-0002-4076-2718>
 Roberto Baraschino  <http://orcid.org/0000-0002-8363-9306>
 Andrea Belleri  <http://orcid.org/0000-0003-2024-7257>
 Donatello Cardone  <http://orcid.org/0000-0002-2814-7456>
 Gaetano Della Corte  <http://orcid.org/0000-0003-2104-3600>
 Paolo Franchin  <http://orcid.org/0000-0002-1995-0415>
 Sergio Lagomarsino  <http://orcid.org/0000-0002-6597-3474>
 Gennaro Magliulo  <http://orcid.org/0000-0002-1812-4357>
 Andrea Marchi  <http://orcid.org/0000-0001-6645-3633>
 Andrea Penna  <http://orcid.org/0000-0001-6457-7827>
 Luciano R.S. Viggiani  <http://orcid.org/0000-0002-8787-8611>
 Alessandro Zona  <http://orcid.org/0000-0002-3100-1802>

References

- Akkar, S., and J. J. Bommer. 2010. Empirical equations for the prediction of PGA, PGV, and spectral accelerations in Europe, the Mediterranean Region, and the Middle East. *Seismological Research Letters* 81 (2):195–206. doi:10.1785/gssrl.81.2.195.
- Ambroseys, N. N., K. A. Simpson, and J. J. Bommer. 1996. Prediction of Horizontal response spectra in Europe. *Earthquake Engineering & Structural Dynamics* 25 (4):371–400. doi:10.1002/(SICI)1096-9845(199604)25:4<371:AID-EQE550>3.0.CO;2-A.
- Ancheta, T. D., R. B. Darragh, J. P. Stewart, E. Seyhan, W. J. Silva, B. S. J. Chiou, K. E. Wooddell, R. W. Graves, A. R. Kottke, D. M. Boore, et al. 2014. NGA-West2 database. *Earthquake Spectra* 30 (3):3. doi:10.1193/070913EQS197M.
- Baker, J. W. 2015. Efficient analytical fragility function fitting using dynamic structural analysis. *Earthquake Spectra* 31 (1):579–99. doi:10.1193/021113EQS025M.
- Baltzopoulos, G., A. Grella, and I. Iervolino. 2021. Seismic reliability implied by behavior-factor-based design. *Earthquake Engineering & Structural Dynamics* 50 (15):4076–4096. doi:10.1002/EQE.3546.
- Barani, S., D. Spallarossa, and P. Bazzurro. 2009. Disaggregation of probabilistic ground-motion hazard in Italy disaggregation of probabilistic ground-motion hazard in Italy. 99 (5):2638–2661. no. September. 10.1785/0120080348.
- Baraschino, R., G. Baltzopoulos, and I. Iervolino. 2020. R2R-EU: Software for fragility fitting and evaluation of estimation uncertainty in seismic risk analysis. *Soil Dynamics and Earthquake Engineering* 132:132. doi:https://doi.org/10.1016/j.soildyn.2020.106093.

- Benjamin, J., and C. A. Cornell, Edited by. 1970. *Probability, statistics, and decision for civil engineers*. New York: McGraw-Hill.
- Bojórquez, E., and I. Iervolino. 2011. Spectral shape proxies and nonlinear structural response. *Soil Dynamics and Earthquake Engineering* 31 (7):996–1008. doi:10.1016/j.soildyn.2011.03.006.
- Cattari, S., D. Camilletti, S. Lagomarsino, S. Bracchi, M. Rota, and A. Penna. 2018. Masonry Italian code-conforming buildings. Part 2: Nonlinear modelling and time-history analysis. *Journal of Earthquake Engineering* 22 (sup2):2010–40. doi:10.1080/13632469.2018.1541030.
- CEN. 2004. Eurocode 8: Design provisions for earthquake resistance of structures, Part 1.1: General Rules, Seismic Actions and Rules for Buildings, EN1998-1.
- Chioccarelli, E., P. Cito, I. Iervolino, and M. Giorgio. 2019. REASSESS V2.0: Software for single- and multi-site probabilistic seismic hazard analysis. *Bulletin of Earthquake Engineering* 17 (4):1769–93. doi:10.1007/s10518-018-00531-x.
- Cito, P., and I. Iervolino. 2020. Peak-over-threshold: Quantifying ground motion beyond design. *Earthquake Engineering & Structural Dynamics* 49 (5):458–78. doi:https://doi.org/10.1002/eqe.3248.
- Cornell, C. A. 1968. Engineering seismic risk analysis. *Bulletin of the Seismological Society of America* 58 (5):1583–1606. doi:10.1785/BSSA0580051583.
- Cornell, C. A., and H. Krawinkler. 2000. Progress and challenges in seismic performance assessment. *PEER Center News* 3 (2):1–3.
- CS.LL.PP. 2008. Norme tecniche per le costruzioni. *Gazzetta Ufficiale Della Repubblica Italiana* 29. (In Italian).
- CS.LL.PP. 2018. Aggiornamento delle norme tecniche per le costruzioni. *Gazzetta Ufficiale Della Repubblica Italiana, GU* 42. (In Italian).
- Dobry, R., I. M. Idriss, and E. Ng. 1978. Duration characteristics of horizontal components of strong-motion earthquake records. *Bulletin of the Seismological Society of America* 68 (5):1487–1520. doi:10.1785/BSSA0680051487.
- FEMA. 2013. *Recommended seismic design criteria for new steel moment-frame buildings: FEMA 350*. Washington, DC, USA: FEMA.
- Franchin, P., L. Ragni, M. Rota, and A. Zona. 2018. Modelling uncertainties of Italian code-conforming structures for the purpose of seismic response analysis. *Journal of Earthquake Engineering* 22 (sup2):1964–89. doi:10.1080/13632469.2018.1527262.
- Gajera, K., B. Dal Lago, L. Capacci, and F. Biondini. 2021. Multi-stripe seismic assessment of precast industrial buildings with cladding panels. *Frontiers in Built Environment* 7 (May):1–15. doi:https://doi.org/10.3389/fbuil.2021.631360.
- Hsiao, P., D. E. Lehman, and C. W. Roeder. 2013. Evaluation of the response modification coefficient and collapse potential of special concentrically braced frames. *Earthquake Engineering & Structural Dynamics* 42 (10):1547–64. doi:https://doi.org/10.1002/eqe.2286.
- Iervolino, I. 2017. Assessing uncertainty in estimation of seismic response for PBEE. *Earthquake Engineering & Structural Dynamics* 46 (10):1711–23. doi:https://doi.org/10.1002/eqe.2883.
- Iervolino, I. 2022. Estimation uncertainty for some common seismic fragility curve fitting methods. *Soil Dynamics and Earthquake Engineering* 152 (August). doi:10.1016/j.soildyn.2021.107068.
- Iervolino, I., and M. Dolce. 2018. Foreword to the special issue for the RINTC (the implicit seismic risk of code-conforming structures) project. *Journal of Earthquake Engineering* 22 (sup2):1–4. doi:10.1080/13632469.2018.1543697.
- Iervolino, I., A. Spillatura, and P. Bazzurro. 2018. Seismic reliability of code-conforming Italian buildings. *Journal of Earthquake Engineering* 22 (sup2):5–27. doi:10.1080/13632469.2018.1540372.
- Jalayer, F., and C. A. Cornell. 2003. A Technical framework for probability-based demand and capacity factor design (DCFD) seismic formats. *PEER Report 2003/8*, 122.
- Lagomarsino, S., A. Penna, A. Galasco, and S. Cattari. 2013. TREMURI program: AN equivalent frame model for the nonlinear seismic analysis of masonry buildings. *Engineering Structures* 56:1787–99. doi:https://doi.org/10.1016/j.engstruct.2013.08.002.
- Lin, T., C. B. Haselton, and J. W. Baker. 2013. Conditional spectrum-based ground motion selection. Part I: Hazard consistency for risk-based assessments. *Earthquake Engineering & Structural Dynamics* 42 (12):1847–65. doi:https://doi.org/10.1002/eqe.2301.
- Luzi, L., S. Hailemichael, D. Bindi, F. Pacor, F. Mele, and F. Sabetta. 2008. ITACA (Italian Accelerometric Archive) : A web portal for the dissemination of Italian strong-motion data. *Seismological Research Letters* 79 (5):716–22. doi:10.1785/gssrl.79.5.716.
- Magliulo, G., D. Bellotti, M. Cimmino, and R. Nascimbene. 2018. Modeling and seismic response analysis of RC precast Italian code-conforming buildings. *Journal of Earthquake Engineering* 22 (sup2):140–67. doi:10.1080/13632469.2018.1531093.
- Magliulo, G., C. Di Salvatore, and M. Ercolino. 2021. Modeling of the beam-to-column dowel connection for a single-story RC precast building. *Frontiers in Built Environment* 7 (2):1–10. doi:https://doi.org/10.3389/fbuil.2021.627546.
- Manzini, C. F., G. Magenes, A. Penna, F. Porto, D. Camilletti, S. Cattari, and S. Lagomarsino. 2018. Masonry Italian code-conforming buildings. Part 1 : Case studies and design methods. *Journal of Earthquake Engineering* 22 (2):54–73. doi:10.1080/13632469.2018.1532358.
- McKenna, F., G. L. Fenves, M. H. Scott, and B. Jeremic. 2000. *Open system for earthquake engineering simulation (opensees)*. CA, USA: Pacific Earthquake Engineering Research Center, University of California.

- Meletti, C., F. Galadini, G. Valensise, M. Stucchi, R. Basili, S. Barba, G. Vannucci, and E. Boschi. 2008. A seismic source zone model for the seismic hazard assessment of the Italian Territory. *Tectonophysics* 450 (1–4):85–108. doi:10.1016/j.tecto.2008.01.003.
- Micozzi, F., A. Flora, L. R. S. Viggiani, D. Cardone, L. Ragni, and A. Dall'Asta. 2021. Risk assessment of reinforced concrete buildings with rubber isolation systems designed by the Italian seismic code. *Accepted for Publication on Journal of Earthquake Engineering*. doi:10.1080/13632469.2021.1961937.
- Monelli, D., M. Pagani, G. Weatherill, V. Silva, and H. Crowley. 2012. The hazard component of OpenQuake: The calculation engine of the Global Earthquake Model. *15th World Conference on Earthquake Engineering, Lisboa 2012*, no. September. 10.13140/2.1.3307.1364.
- Ponzo, F. C., A. Di Cesare, A. Telesca, A. Pavese, and M. Furinghetti. 2021. Advanced modelling and risk analysis of RC buildings with sliding isolation systems designed by the Italian seismic code. *Applied Sciences (Switzerland)* 11 (4):1–16. doi:10.3390/app11041938.
- Ragni, L., D. Cardone, N. Conte, A. Dall'Asta, A. Di Cesare, A. Flora, G. Leccese, F. Micozzi, and F. C. Ponzo. 2018. Modelling and seismic response analysis of Italian code-conforming base-isolated buildings. *Journal of Earthquake Engineering* 22 (sup2):198–230. doi:10.1080/13632469.2018.1527263.
- Ricci, P., V. Manfredi, F. Noto, M. Terrenzi, C. Petrone, F. Celano, M. T. De Risi, G. Camata, P. Franchin, G. Magliulo, et al. 2018. Modeling and seismic response analysis of Italian code-conforming reinforced concrete buildings. *Journal of Earthquake Engineering* 22 (sup2):105–39. doi:https://doi.org/10.1080/13632469.2018.1527733.
- RINTC-Workgroup. 2018. Results of the 2015–2017 implicit seismic risk of code-conforming structures in Italy (RINTC) project. *ReLUIIS Report, Rete Dei Laboratori Universitari Di Ingegneria Sismica (ReLUIIS) Naples, Italy*.
- Romão, X., R. Delgado, and A. Costa. 2014. Probabilistic performance analysis of existing buildings under earthquake loading. *Journal of Earthquake Engineering* 18 (8):1241–65. doi:10.1080/13632469.2014.937015.
- Scozzese, F., G. Terracciano, A. Zona, G. Della Corte, A. Dall'Asta, and R. Landolfo. 2018. Modeling and seismic response analysis of Italian code-conforming single-storey steel buildings modeling and seismic response analysis of Italian. *Journal of Earthquake Engineering* 22 (2):168–97. doi:10.1080/13632469.2018.1528913.
- Shome, N., and C. A. Cornell. 2000. Structural seismic demand analysis: Consideration of “collapse.” In *8th ACSE Specialty Conference on Probabilistic Mechanics and Structural Reliability*, PMC2000–119. South Bend, Indiana, USA.
- Shome, N., C. A. Cornell, P. Bazzurro, and J. E. Carballo. 1998. Earthquakes, records, and nonlinear responses. *Earthquake Spectra* 14 (3):469–500. doi:10.1193/1.1586011.
- Skoulidou, D., and X. Romão. 2019. Uncertainty quantification of fragility and risk estimates due to seismic input variability and capacity model uncertainty. *Engineering Structures* 195:425–37. doi:10.1016/j.engstruct.2019.05.067.
- Spillatura, A., M. Kohrangi, P. Bazzurro, and D. Vamvatsikos. 2021. Conditional spectrum record selection faithful to causative earthquake parameter distributions. *Earthquake Engineering & Structural Dynamics* 50 (10):2653–2671. doi:https://doi.org/10.1002/eqe.3465.
- Suzuki, A., and I. Iervolino. 2020. Intensity measure conversion of fragility curves. *Earthquake Engineering & Structural Dynamics* 49 (6):6. doi:https://doi.org/10.1002/eqe.3256.
- Suzuki, A., and I. Iervolino. 2021. Seismic fragility of code-conforming Italian buildings based on SDoF approximation. *Journal of Earthquake Engineering* 25 (14):2873–2907. doi:10.1080/13632469.2019.1657989.
- Vamvatsikos, D., and C. A. Cornell. 2002. Incremental dynamic analysis. *Earthquake Engineering & Structural Dynamics* 31 (3):491–514. doi:https://doi.org/10.1002/eqe.141.
- Vamvatsikos, D., and C. A. Cornell. 2005. Developing efficient scalar and vector intensity measures for IDA capacity estimation by incorporating elastic spectral shape information. *Earthquake Engineering & Structural Dynamics* 34 (13):1573–1600. doi:https://doi.org/10.1002/eqe.496.

Appendix

Fitting results are given in Tables 5–9, for all the buildings belonging to the investigated structural typologies (URM, RC, BI, PRC, and S, respectively), via the following information:

- *ID-building* containing fundamental information to identify the structure, such as typology, number of floors, site and soil condition;
- *Failure criteria* identifies one between Global Collapse (GC) and usability-preventing damage (UPD);
- *Curve fitting method* is the method used to evaluate the parameters of lognormal fragility;
- IM is the intensity measure respect of which fragility curves are evaluated;
- η is the mean of the logarithms of the IM causing structural failure;
- β is the standard deviation of the logarithms of the IM causing structural failure;
- λ_f identifies the failure rate;
- $CoV[\lambda_f]$ is the coefficient of variation of the failure rate.
- LFM is the maximum values of the lumped fragility.

Table 5. URM buildings.

| ID-building | Failure criteria | Curve fitting method | IM | η | β | λ_r | CoV [M_r] | LFM |
|----------------|------------------|----------------------|-----------|--------|---------|-------------|---------------|----------|
| URM-C1-2-AQ-A | GC | LSF | Sa(0.15s) | 0.341 | 0.370 | 3.41E-04 | 0.211 | 0.92 |
| | UPD | LSF | Sa(0.15s) | -0.795 | 0.330 | 5.69E-03 | 0.197 | 1 |
| URM-C1-2-MI-A | GC | GPP | Sa(0.15s) | 4.241 | 0.486 | 5.35E-20 | 6.252 | 5.40E-15 |
| | UPD | GPP | Sa(0.15s) | -0.688 | 0.365 | 2.84E-05 | 1.161 | 0.039 |
| URM-C1-2-MI-C | GC | GPP | Sa(0.15s) | -0.452 | 0.084 | 5.23E-06 | 1.085 | 1.09E-11 |
| | UPD | GPP | Sa(0.15s) | -1.164 | 0.091 | 1.79E-04 | 0.482 | 0.099 |
| URM-C1-2-NA-A* | GC | ML | Sa(0.15s) | 0.765 | 0.468 | 1.93E-05 | 0.473 | 0.30 |
| | UPD | LSF | Sa(0.15s) | -0.766 | 0.335 | 1.60E-03 | 0.195 | 1 |
| URM-C1-2-NA-C | GC | LSF | Sa(0.15s) | 0.946 | 0.421 | 1.53E-05 | 0.608 | 0.31 |
| | UPD | LSF | Sa(0.15s) | -0.719 | 0.245 | 2.03E-03 | 0.116 | 1 |
| URM-C1-3-AQ-A | GC | LSF | Sa(0.15s) | 0.231 | 0.463 | 6.00E-04 | 0.282 | 0.9 |
| | UPD | LSF | Sa(0.15s) | -1.048 | 0.222 | 8.83E-03 | 0.115 | 1 |
| URM-C1-3-NA-A* | GC | LSF | Sa(0.15s) | 0.654 | 0.485 | 3.25E-05 | 0.603 | 0.45 |
| | UPD | LSF | Sa(0.15s) | -1.033 | 0.236 | 2.70E-03 | 0.113 | 1 |
| URM-C2-2-NA-C* | GC | LSF | Sa(0.15s) | 0.875 | 0.390 | 1.68E-05 | 1.041 | 0.36 |
| | UPD | LSF | Sa(0.15s) | -0.702 | 0.265 | 2.01E-03 | 0.128 | 1 |
| URM-C2-3-MI-A | GC | GPP | Sa(0.15s) | -0.364 | 0.104 | 1.10E-06 | 2.098 | 2.28E-16 |
| | UPD | GPP | Sa(0.15s) | -0.989 | 0.220 | 4.86E-05 | 0.269 | 0.50 |
| URM-C2-3-MI-C | GC | GPP | Sa(0.15s) | -0.057 | 0.120 | 6.01E-07 | 1.273 | 2.23E-09 |
| | UPD | LSF | Sa(0.15s) | -0.860 | 0.309 | 1.03E-04 | 0.321 | 0.57 |
| URM-C3-2-AQ-A* | GC | ML | Sa(0.15s) | 0.480 | 0.317 | 2.01E-04 | 0.169 | 0.95 |
| | UPD | LSF | Sa(0.15s) | -0.718 | 0.336 | 4.80E-03 | 0.248 | 1 |
| URM-C3-2-AQ-C | GC | LSF | Sa(0.15s) | 0.515 | 0.282 | 2.93E-04 | 0.153 | 1 |
| | UPD | LSF | Sa(0.15s) | -0.551 | 0.308 | 4.89E-03 | 0.189 | 1 |
| URM-C3-2-NA-A | GC | LSF | Sa(0.15s) | 0.733 | 0.340 | 1.01E-05 | 0.371 | 0.34 |
| | UPD | GPP | Sa(0.15s) | -0.879 | 0.323 | 2.09E-03 | 0.362 | 1 |
| URM-C3-3-NA-C | GC | LSF | Sa(0.15s) | 0.694 | 0.453 | 4.79E-05 | 0.411 | 0.53 |
| | UPD | LSF | Sa(0.15s) | -0.873 | 0.277 | 3.11E-03 | 0.115 | 1 |
| URM-C4-2-MI-A | GC | GPP | Sa(0.15s) | 2.045 | 0.298 | 1.20E-13 | 5.378 | 1.61E-14 |
| | UPD | GPP | Sa(0.15s) | -0.434 | 0.409 | 1.24E-05 | 1.820 | 0.044 |
| URM-C4-2-NA-C | GC | LSF | Sa(0.15s) | 0.955 | 0.349 | 9.52E-06 | 0.323 | 0.27 |
| | UPD | ML | Sa(0.15s) | -0.572 | 0.311 | 1.54E-03 | 0.174 | 1 |
| URM-C4-3-NA-A | GC | LSF | Sa(0.15s) | 0.694 | 0.459 | 2.41E-05 | 0.481 | 0.41 |
| | UPD | LSF | Sa(0.15s) | -0.956 | 0.324 | 2.54E-03 | 0.161 | 1 |
| URM-C5-3-NA-C | GC | LSF | Sa(0.15s) | 0.729 | 0.417 | 3.45E-05 | 0.367 | 0.50 |
| | UPD | LSF | Sa(0.15s) | -0.856 | 0.245 | 2.87E-03 | 0.108 | 1 |
| URM-C5-3-NA-C* | GC | ML | Sa(0.15s) | 0.616 | 0.390 | 4.58E-05 | 0.336 | 0.60 |
| | UPD | LSF | Sa(0.15s) | -0.856 | 0.245 | 2.87E-03 | 0.107 | 1 |
| URM-C6-3-MI-A | GC | GPP | Sa(0.15s) | -0.228 | 0.127 | 5.35E-07 | 2.317 | 5.72E-21 |
| | UPD | GPP | Sa(0.15s) | -1.205 | 0.191 | 1.17E-04 | 0.532 | 0.15 |

(Continued)



Table 5. (Continued).

| ID-building | Failure criteria | Curve fitting method | IM | η | β | λ_r | $CoV[\lambda_r]$ | LFM |
|----------------|------------------|----------------------|-----------|--------|---------|-------------|------------------|----------|
| URM-C7-2-MI-C | GC | GPP | Sa(0.15s) | -0.178 | 0.079 | 1.08E-06 | 1.435 | 5.25E-24 |
| | UPD | GPP | Sa(0.15s) | -0.834 | 0.127 | 4.18E-05 | 0.651 | 0.013 |
| URM-11-2-AQ-A* | GC | GPP | Sa(0.15s) | 0.113 | 0.249 | 4.89E-04 | 0.185 | 1 |
| | UPD | LSF | Sa(0.15s) | -1.061 | 0.354 | 1.09E-02 | 0.202 | 1 |
| URM-11-2-AQ-C | GC | ML | Sa(0.15s) | 0.073 | 0.236 | 9.03E-04 | 0.130 | 1 |
| | UPD | GPP | Sa(0.15s) | -1.046 | 0.409 | 1.76E-02 | 0.385 | 1 |
| URM-11-2-NA-C* | GC | LSF | Sa(0.15s) | 0.205 | 0.225 | 1.11E-04 | 0.176 | 0.99 |
| | UPD | LSF | Sa(0.15s) | -0.940 | 0.320 | 3.88E-03 | 0.140 | 1 |
| URM-12-3-NA-A* | GC | LSF | Sa(0.15s) | 0.315 | 0.484 | 1.05E-04 | 0.392 | 0.69 |
| | UPD | LSF | Sa(0.15s) | -1.389 | 0.455 | 8.21E-03 | 0.251 | 1 |
| URM-12-3-NA-C | GC | LSF | Sa(0.15s) | 0.480 | 0.456 | 1.02E-04 | 0.297 | 0.68 |
| | UPD | LSF | Sa(0.15s) | -1.134 | 0.302 | 5.85E-03 | 0.158 | 1 |
| URM-E2-2-AQ-A | GC | LSF | Sa(0.15s) | 0.681 | 0.559 | 3.14E-04 | 0.291 | 0.81 |
| | UPD | LSF | Sa(0.15s) | -0.057 | 0.302 | 1.16E-03 | 0.161 | 1 |
| URM-E2-2-AQ-C | GC | LSF | Sa(0.15s) | 0.602 | 0.342 | 3.27E-04 | 0.219 | 0.98 |
| | UPD | LSF | Sa(0.15s) | -0.041 | 0.207 | 1.52E-03 | 0.115 | 1 |
| URM-E2-2-MI-A | GC | LSF | Sa(0.15s) | 0.956 | 0.167 | 6.94E-37 | 6.674 | 9.33E-32 |
| | UPD | LSF | Sa(0.15s) | 0.180 | 0.200 | 2.47E-13 | 18.948 | 1.20E-11 |
| URM-E2-2-MI-C | GC | LSF | Sa(0.15s) | 0.296 | 0.124 | 1.33E-24 | 21.067 | 5.24E-18 |
| | UPD | LSF | Sa(0.15s) | 0.062 | 0.165 | 5.70E-12 | 4.662 | 1.49E-05 |
| URM-E2-3-AQ-A | GC | LSF | Sa(0.15s) | 0.424 | 0.535 | 5.74E-04 | 0.289 | 0.88 |
| | UPD | LSF | Sa(0.15s) | -0.243 | 0.421 | 2.45E-03 | 0.151 | 1 |
| URM-E2-3-MI-A | GC | LSF | Sa(0.15s) | -0.523 | 0.082 | 4.41E-14 | 16.124 | 2.00E-09 |
| | UPD | LSF | Sa(0.15s) | -0.725 | 0.106 | 5.97E-07 | 0.978 | 0.0066 |
| URM-E2-3-MI-C | GC | LSF | Sa(0.15s) | -0.415 | 0.081 | 3.35E-12 | 3.597 | 7.47E-09 |
| | UPD | LSF | Sa(0.15s) | -0.380 | 0.196 | 1.33E-06 | 2.129 | 0.015 |
| URM-E2-3-NA-C | GC | LSF | Sa(0.15s) | 0.877 | 0.245 | 1.12E-05 | 0.348 | 0.29 |
| | UPD | LSF | Sa(0.15s) | -0.065 | 0.571 | 1.29E-03 | 0.224 | 0.91 |
| URM-E5-2-AQ-C | GC | LSF | Sa(0.15s) | 0.557 | 0.427 | 4.69E-04 | 0.260 | 0.95 |
| | UPD | LSF | Sa(0.15s) | -0.324 | 0.261 | 3.43E-03 | 0.142 | 1 |
| URM-E5-2-MI-A | GC | LSF | Sa(0.15s) | 1.216 | 0.206 | 3.96E-32 | 21.378 | 6.66E-29 |
| | UPD | LSF | Sa(0.15s) | -0.162 | 0.211 | 4.02E-09 | 1.583 | 8.47E-08 |
| URM-E5-3-MI-A | GC | LSF | Sa(0.15s) | -0.652 | 0.096 | 1.79E-09 | 1.492 | 1.67E-10 |
| | UPD | LSF | Sa(0.15s) | -1.286 | 0.243 | 1.66E-04 | 0.166 | 0.91 |
| URM-E5-3-NA-A | GC | LSF | Sa(0.15s) | 0.658 | 0.622 | 1.18E-04 | 0.461 | 0.44 |
| | UPD | LSF | Sa(0.15s) | -1.282 | 0.323 | 7.82E-03 | 0.111 | 1 |
| URM-E8-2-AQ-C | GC | LSF | Sa(0.15s) | 0.611 | 0.321 | 3.01E-04 | 0.229 | 1 |
| | UPD | LSF | Sa(0.15s) | -0.249 | 0.199 | 2.57E-03 | 0.115 | 1 |
| URM-E8-2-NA-A | GC | LSF | Sa(0.15s) | 0.842 | 0.408 | 1.75E-05 | 0.723 | 0.27 |
| | UPD | LSF | Sa(0.15s) | -0.173 | 0.266 | 4.44E-04 | 0.126 | 0.88 |

(Continued)

Table 5. (Continued).

| ID-building | Failure criteria | Curve fitting method | IM | η | β | λ_r | CoV(λ_r) | LFM |
|---------------|------------------|----------------------|-----------|--------|---------|-------------|--------------------|---------|
| URM-E8-3-AQ-A | GC | LSF | Sa(0.15s) | 0.468 | 0.514 | 4.72E-04 | 0.239 | 0.90 |
| | UPD | LSF | Sa(0.15s) | -0.258 | 0.382 | 2.32E-03 | 0.173 | 1 |
| URM-E8-3-MI-C | GC | LSF | Sa(0.15s) | -0.389 | 0.131 | 7.37E-09 | 2.364 | 0.00059 |
| | UPD | LSF | Sa(0.15s) | -0.641 | 0.147 | 1.17E-05 | 0.571 | 0.13 |
| URM-E8-3-NA-C | GC | LSF | Sa(0.15s) | 0.865 | 0.323 | 2.04E-05 | 1.214 | 0.35 |
| | UPD | LSF | Sa(0.15s) | -0.115 | 0.508 | 1.12E-03 | 0.178 | 0.95 |
| URM-E9-2-AQ-C | GC | LSF | Sa(0.15s) | 0.279 | 0.262 | 6.67E-04 | 0.178 | 0.95 |
| | UPD | LSF | Sa(0.15s) | -0.111 | 0.178 | 1.75E-03 | 0.095 | 1 |
| URM-E9-3-MI-C | GC | LSF | Sa(0.15s) | -0.634 | 0.094 | 3.56E-07 | 1.193 | 0.032 |
| | UPD | LSF | Sa(0.15s) | -0.763 | 0.098 | 2.93E-05 | 0.303 | 0.32 |

Table 6. RC buildings.

| ID-building | Failure criteria | Curve fitting method | IM | η | β | λ_r | $CoV[\lambda_r]$ | LFM |
|-----------------|------------------|----------------------|-----------|--------|---------|-------------|------------------|----------|
| RC-BF-9-AQ-A | GC | LSF | Sa(2.0s) | -0.461 | 0.317 | 2.31E-05 | 0.297 | 0.68 |
| | UPD | LSF | Sa(2.0s) | -2.725 | 0.271 | 3.00E-03 | 0.107 | 1 |
| RC-IF-9-AQ-A | GC | LSF | Sa(1.0s) | 0.582 | 0.367 | 6.71E-06 | 0.370 | 0.68 |
| | UPD | ML | Sa(1.0s) | -1.426 | 0.225 | 6.62E-04 | 0.110 | 1 |
| RC-PF-9-AQ-A | GC | ML | Sa(1.0s) | 0.604 | 0.362 | 6.18E-06 | 0.259 | 0.65 |
| | UPD | LSF | Sa(1.0s) | -1.460 | 0.162 | 6.79E-04 | 0.073 | 1 |
| RC-BF-3-AQ-C | GC | LSF | Sa(1.0s) | 1.805 | 0.702 | 1.37E-05 | 0.991 | 0.22 |
| | UPD | LSF | Sa(1.0s) | -1.627 | 0.576 | 7.66E-03 | 0.162 | 1 |
| RC-IF-3-AQ-C | GC | LSF | Sa(0.15s) | 1.791 | 0.661 | 2.91E-05 | 0.747 | 0.32 |
| | UPD | LSF | Sa(0.15s) | -0.438 | 0.414 | 4.58E-03 | 0.186 | 1 |
| RC-PF-3-AQ-C | GC | LSF | Sa(0.5s) | 1.748 | 0.465 | 4.45E-05 | 0.359 | 0.73 |
| | UPD | LSF | Sa(0.5s) | -0.017 | 0.265 | 1.33E-03 | 0.089 | 1 |
| RC-BF-6-AQ-C | GC | LSF | Sa(1.5s) | 0.526 | 0.365 | 2.97E-05 | 0.319 | 0.71 |
| | UPD | GPP | Sa(1.5s) | -2.261 | 0.388 | 6.50E-03 | 0.136 | 1 |
| RC-IF-6-AQ-C | GC | ML | Sa(0.5s) | 1.498 | 0.670 | 1.35E-04 | 0.333 | 0.75 |
| | UPD | ML | Sa(0.5s) | -0.330 | 0.388 | 2.64E-03 | 0.147 | 1 |
| RC-PF-6-AQ-C | GC | LSF | Sa(0.5s) | 1.479 | 0.754 | 1.77E-04 | 0.360 | 0.75 |
| | UPD | ML | Sa(0.5s) | -0.280 | 0.327 | 2.26E-03 | 0.120 | 1 |
| RC-SW-BF-9-AQ-C | GC | LSF | Sa(1.5s) | 1.051 | 0.312 | 5.73E-06 | 0.288 | 0.15 |
| | UPD | LSF | Sa(1.5s) | -2.270 | 0.332 | 6.27E-03 | 0.109 | 1 |
| RC-SW-IF-9-AQ-C | GC | LSF | Sa(1.0s) | 1.430 | 0.613 | 2.53E-05 | 0.516 | 0.39 |
| | UPD | LSF | Sa(1.0s) | -1.560 | 0.379 | 5.45E-03 | 0.152 | 1 |
| RC-SW-PF-9-AQ-C | GC | LSF | Sa(1.0s) | 1.555 | 0.577 | 1.60E-05 | 0.597 | 0.30 |
| | UPD | LSF | Sa(1.0s) | -1.714 | 0.423 | 7.26E-03 | 0.149 | 1 |
| RC-BF-3-MI-C | GC | ML | Sa(1.0s) | 4.373 | 2.649 | 1.19E-04 | 1.207 | 0.05 |
| | UPD | LSF | Sa(1.0s) | -1.841 | 0.439 | 2.58E-04 | 0.240 | 0.85 |
| RC-IF-3-MI-C | GC | LSF | Sa(0.15s) | 0.303 | 0.318 | 3.06E-07 | 2.112 | 3.56E-05 |
| | UPD | LSF | Sa(0.15s) | 0.060 | 0.515 | 8.45E-06 | 1.515 | 0.05 |
| RC-PF-3-MI-C | GC | GPP | Sa(0.5s) | 1.694 | 0.394 | 5.97E-10 | 4.376 | 7.07E-09 |
| | UPD | LSF | Sa(0.5s) | -0.508 | 0.354 | 2.40E-05 | 0.267 | 0.34 |
| RC-SW-BF-9-MI-C | GC | GPP | Sa(2.0s) | 2.419 | 0.302 | 3.73E-19 | 9.417 | 4.87E-48 |
| | UPD | LSF | Sa(2.0s) | -2.373 | 0.160 | 3.26E-05 | 0.185 | 0.90 |
| RC-SW-IF-9-MI-C | GC | GPP | Sa(1.0s) | 2.269 | 0.344 | 2.17E-14 | 9.494 | 2.09E-13 |
| | UPD | LSF | Sa(1.0s) | -1.140 | 0.249 | 9.51E-06 | 0.246 | 0.25 |
| RC-SW-PF-9-MI-C | GC | GPP | Sa(1.0s) | 0.490 | 0.208 | 1.39E-09 | 2.477 | 3.62E-20 |
| | UPD | LSF | Sa(1.0s) | -1.111 | 0.358 | 1.40E-05 | 0.355 | 0.29 |
| RC-BF-6-MI-C | GC | GPP | Sa(1.5s) | 1.225 | 0.215 | 4.07E-14 | 8.186 | 3.36E-44 |
| | UPD | LSF | Sa(1.5s) | -2.442 | 0.207 | 1.41E-04 | 0.199 | 1 |
| RC-IF-6-MI-C | GC | LSF | Sa(0.5s) | 0.400 | 0.309 | 3.29E-07 | 0.792 | 1.09E-05 |
| | UPD | LSF | Sa(0.5s) | -0.547 | 0.290 | 2.07E-05 | 0.249 | 0.36 |
| RC-PF-6-MI-C | GC | GPP | Sa(0.5s) | 1.427 | 0.464 | 7.34E-09 | 6.574 | 1.68E-05 |
| | UPD | ML | Sa(0.5s) | -0.417 | 0.599 | 7.20E-05 | 0.709 | 0.40 |

(Continued)

Table 6. (Continued).

| ID-building | Failure criteria | Curve fitting method | IM | η | β | λ_r | CoV [λ_r] | LFM |
|---------------------|------------------|----------------------|-----------|--------|---------|-------------|---------------------|----------|
| RC-BF-9-MI-C | GC | GPP | Sa(2.0s) | 3.183 | 0.277 | 1.96E-23 | 14.116 | 9.84E-42 |
| | UPD | ML | Sa(2.0s) | -2.539 | 0.257 | 8.24E-05 | 0.241 | 0.95 |
| RC-IF-9-MI-C | GC | GPP | Sa(1.0s) | 4.732 | 0.721 | 1.59E-17 | 12.532 | 4.05E-13 |
| | UPD | LSF | Sa(1.0s) | -1.417 | 0.186 | 2.38E-05 | 0.366 | 0.73 |
| RC-PF-9-MI-C | GC | GPP | Sa(1.0s) | -0.162 | 0.143 | 4.89E-08 | 1.579 | 1.06E-17 |
| | UPD | LSF | Sa(1.0s) | -1.402 | 0.344 | 3.96E-05 | 0.333 | 0.61 |
| RC-BF-3-NA-C | GC | GPP | Sa(1.0s) | 7.020 | 0.687 | 5.14E-22 | 21.236 | 1.27E-11 |
| | UPD | ML | Sa(1.0s) | -1.866 | 0.430 | 5.11E-03 | 0.178 | 1 |
| RC-IF-3-NA-C | GC | LSF | Sa(0.15s) | 1.411 | 0.322 | 9.53E-07 | 3.988 | 0.02 |
| | UPD | GPP | Sa(0.15s) | -0.076 | 0.512 | 6.84E-04 | 0.211 | 0.84 |
| RC-PF-3-NA-C | GC | ML | Sa(0.5s) | 3.441 | 1.367 | 8.70E-06 | 2.357 | 0.05 |
| | UPD | LSF | Sa(0.5s) | -0.511 | 0.437 | 1.35E-03 | 0.146 | 0.99 |
| RC-BF-6-NA-C | GC | GPP | Sa(1.5s) | 1.498 | 0.357 | 7.25E-10 | 4.213 | 9.94E-10 |
| | UPD | ML | Sa(1.5s) | -2.262 | 0.362 | 3.42E-03 | 0.177 | 1 |
| RC-IF-6-NA-C | GC | LSF | Sa(0.5s) | 1.329 | 0.235 | 1.55E-06 | 0.613 | 0.01 |
| | UPD | LSF | Sa(0.5s) | -1.108 | 0.494 | 2.57E-04 | 0.353 | 1 |
| RC-PF-6-NA-C | GC | LSF | Sa(0.5s) | 1.887 | 0.397 | 3.42E-07 | 1.070 | 2.07E-03 |
| | UPD | ML | Sa(0.5s) | -1.420 | 0.480 | 5.85E-04 | 0.356 | 1 |
| RC-BF-9-NA-C | GC | ML | Sa(2.0s) | 4.343 | 2.462 | 4.43E-05 | 1.243 | 0.05 |
| | UPD | LSF | Sa(2.0s) | -2.757 | 0.355 | 4.27E-03 | 0.147 | 1 |
| RC-IF-9-NA-C | GC | ML | Sa(1.0s) | 2.782 | 1.384 | 8.25E-06 | 1.666 | 0.05 |
| | UPD | ML | Sa(1.0s) | -1.507 | 0.160 | 1.73E-03 | 0.093 | 1 |
| RC-PF-9-NA-C | GC | ML | Sa(1.0s) | 0.756 | 0.702 | 1.43E-05 | 1.301 | 0.15 |
| | UPD | LSF | Sa(1.0s) | -1.447 | 0.243 | 1.63E-03 | 0.123 | 1 |
| RC-SW-BF-9-NA-C | GC | GPP | Sa(1.5s) | 1.530 | 0.185 | 7.76E-11 | 5.027 | 1.11E-11 |
| | UPD | LSF | Sa(1.5s) | -2.110 | 0.239 | 2.08E-03 | 0.140 | 1 |
| RC-SW-IF-9-NA-C | GC | GPP | Sa(1.0s) | 8.298 | 0.653 | 1.71E-29 | 19.504 | 1.51E-14 |
| | UPD | LSF | Sa(1.0s) | -1.130 | 0.202 | 6.70E-04 | 0.103 | 1 |
| RC-SW-PF-9-NA-C | GC | GPP | Sa(1.0s) | 5.220 | 0.433 | 1.06E-20 | 7.855 | 1.35E-16 |
| | UPD | ML | Sa(1.0s) | -1.190 | 0.168 | 7.60E-04 | 0.105 | 1 |
| RC-MU-BF-6-NA-C | GC | GPP | Sa(1.5s) | 1.585 | 0.509 | 3.90E-09 | 4.737 | 4.03E-04 |
| | UPD | GPP | Sa(1.5s) | -2.122 | 0.298 | 2.25E-03 | 0.188 | 1 |
| RC-MU-IF-6-NA-C | GC | GPP | Sa(0.5s) | 2.621 | 0.770 | 5.14E-07 | 1.234 | 4.25E-03 |
| | UPD | LSF | Sa(0.5s) | -0.890 | 0.667 | 4.87E-03 | 0.228 | 0.98 |
| RC-MU-PF-6-NA-C | GC | LSF | Sa(0.5s) | 6.187 | 2.115 | 6.12E-06 | 1.635 | 4.67E-03 |
| | UPD | GPP | Sa(0.5s) | -0.436 | 0.600 | 1.68E-03 | 0.176 | 0.98 |
| RC-SSI-SW-BF-9-NA-C | GC | LSF | Sa(1.0s) | 4.117 | 1.394 | 6.66E-08 | 2.546 | 2.22E-04 |
| | UPD | ML | Sa(1.0s) | -2.679 | 0.549 | 1.18E-02 | 0.192 | 1 |
| RC-SSI-SW-IF-9-NA-C | GC | LSF | Sa(1.0s) | 4.003 | 1.459 | 1.92E-07 | 2.043 | 9.25E-04 |
| | UPD | ML | Sa(1.0s) | -2.180 | 0.270 | 3.84E-03 | 0.117 | 1 |
| RC-SSI-SW-PF-9-NA-C | GC | LSF | Sa(1.0s) | 3.062 | 1.108 | 5.72E-08 | 2.480 | 4.13E-04 |
| | UPD | ML | Sa(1.0s) | -2.283 | 0.241 | 4.64E-03 | 0.127 | 1 |

Table 7. BI buildings.

| ID-building | Failure criteria | Curve fitting method | IM | η | β | λ_f | $CoV[\lambda_f]$ | LFM |
|-------------------|------------------|----------------------|----------|--------|---------|-------------|------------------|------|
| BI-FPS-AQ-C | GC | ML | Sa(3.0s) | -1.435 | 0.250 | 4.34E-04 | 0.137 | 1 |
| | UPD | ML | Sa(3.0s) | -1.510 | 0.370 | 5.95E-04 | 0.177 | 1 |
| BI-FPS-NA-C | GC | LSF | Sa(3.0s) | -1.474 | 0.088 | 3.94E-05 | 0.092 | 1 |
| | UPD | LSF | Sa(3.0s) | -1.427 | 0.176 | 3.66E-05 | 0.192 | 0.98 |
| BI-HDRB+SLDR-AQ-C | GC | ML | Sa(3.0s) | -1.306 | 0.189 | 3.02E-04 | 0.127 | 1 |
| | UPD | ML | Sa(3.0s) | -1.551 | 0.349 | 6.34E-04 | 0.161 | 1 |
| BI-HDRB+SLDR-NA-C | GC | ML | Sa(3.0s) | -1.501 | 0.238 | 5.78E-05 | 0.169 | 1 |
| | UPD | ML | Sa(3.0s) | -1.614 | 0.199 | 7.55E-05 | 0.138 | 1 |
| BI-HDRB-AQ-C | GC | ML | Sa(3.0s) | -1.214 | 0.287 | 2.70E-04 | 0.163 | 1 |
| | UPD | ML | Sa(3.0s) | -1.774 | 0.437 | 1.11E-03 | 0.188 | 1 |
| BI-HDRB-NA-C | GC | D* | Sa(3.0s) | -1.221 | 0.143 | 1.31E-05 | 0.190 | 0.90 |
| | UPD | ML | Sa(3.0s) | -1.537 | 0.166 | 5.49E-05 | 0.121 | 1 |

*D = means that fragility parameters are assigned, without a numerical fitting procedure. For uncertainty estimation, in this case, the parameters of each fragility function from each resampling, was by means LSF method.

Table 8. PRC buildings. $CoV[\lambda_f] = NaN$ means that resampling procedure does not provide results. This may happen when collapses/ failures occur only for few records in a single stripe.

| ID-building | Failure criteria | Curve fitting method | IM | η | β | λ_f | $CoV[\lambda_f]$ | LFM |
|----------------|------------------|----------------------|----------|--------|---------|-------------|------------------|----------|
| PRC-Geom1-AQ-A | GC | ML | Sa(2.0s) | -0.709 | 0.237 | 3.97E-05 | 0.181 | 0.95 |
| | UPD | ML | Sa(2.0s) | -2.513 | 0.042 | 1.88E-03 | NaN | 1 |
| PRC-Geom2-AQ-A | GC | ML | Sa(2.0s) | -0.322 | 0.068 | 1.02E-05 | NaN | 0.55 |
| | UPD | ML | Sa(2.0s) | -2.543 | 0.317 | 2.25E-03 | 0.121 | 1 |
| PRC-Geom3-AQ-A | GC | ML | Sa(2.0s) | -0.295 | 0.071 | 9.36E-06 | NaN | 0.40 |
| | UPD | ML | Sa(2.0s) | -2.363 | 0.276 | 1.62E-03 | 0.118 | 1 |
| PRC-Geom4-AQ-A | GC | ML | Sa(2.0s) | -0.286 | 0.072 | 9.07E-06 | NaN | 0.35 |
| | UPD | ML | Sa(2.0s) | -2.385 | 0.259 | 1.66E-03 | 0.111 | 1 |
| PRC-Geom1-AQ-C | GC | ML | Sa(2.0s) | -0.570 | 0.044 | 7.08E-05 | NaN | 1 |
| | UPD | ML | Sa(2.0s) | -2.438 | 0.312 | 3.93E-03 | 0.125 | 1 |
| PRC-Geom2-AQ-C | GC | ML | Sa(2.0s) | 0.083 | 0.068 | 1.07E-05 | NaN | 0.45 |
| | UPD | ML | Sa(2.0s) | -2.512 | 0.338 | 4.41E-03 | 0.139 | 1 |
| PRC-Geom3-AQ-C | GC | ML | Sa(2.0s) | 0.152 | 0.075 | 8.55E-06 | NaN | 0.15 |
| | UPD | ML | Sa(2.0s) | -2.202 | 0.449 | 3.05E-03 | 0.177 | 1 |
| PRC-Geom4-AQ-C | GC | ML | Sa(2.0s) | 0.083 | 0.068 | 1.07E-05 | NaN | 0.45 |
| | UPD | ML | Sa(2.0s) | -2.290 | 0.392 | 3.31E-03 | 0.155 | 1 |
| PRC-Geom1-MI-A | GC | LSF | Sa(2.0s) | 22.780 | 7.167 | 8.08E-07 | 0.668 | 1.69E-14 |
| | UPD | LSF | Sa(2.0s) | -1.461 | 0.582 | 1.79E-06 | 1.014 | 0.02 |
| PRC-Geom2-MI-A | GC | LSF | Sa(2.0s) | 22.780 | 7.167 | 8.08E-07 | 0.873 | 3.30E-14 |
| | UPD | LSF | Sa(2.0s) | -1.438 | 0.582 | 1.63E-06 | 0.894 | 0.02 |
| PRC-Geom3-MI-A | GC | GPP | Sa(2.0s) | -0.195 | 0.265 | 3.22E-11 | 5.996 | 4.02E-19 |
| | UPD | LSF | Sa(2.0s) | -1.902 | 0.223 | 7.47E-07 | 1.200 | 6.44E-04 |
| PRC-Geom4-MI-A | GC | GPP | Sa(2.0s) | -1.113 | 0.251 | 1.17E-08 | 3.483 | 7.94E-09 |
| | UPD | LSF | Sa(2.0s) | -2.009 | 0.225 | 1.28E-06 | 0.983 | 3.45E-03 |
| PRC-Geom1-MI-C | GC | GPP | Sa(2.0s) | 13.283 | 1.749 | 6.14E-23 | 21.401 | 3.95E-10 |
| | UPD | ML | Sa(2.0s) | -2.172 | 0.050 | 1.18E-05 | NaN | 0.50 |
| PRC-Geom2-MI-C | GC | GPP | Sa(2.0s) | 3.544 | 0.705 | 6.61E-17 | 14.078 | 7.11E-12 |
| | UPD | ML | Sa(2.0s) | -2.184 | 0.049 | 1.22E-05 | NaN | 0.60 |
| PRC-Geom3-MI-C | GC | GPP | Sa(2.0s) | -0.880 | 0.202 | 2.40E-08 | 2.223 | 4.41E-06 |
| | UPD | GPP | Sa(2.0s) | -2.213 | 0.152 | 1.65E-05 | 0.566 | 0.69 |
| PRC-Geom4-MI-C | GC | GPP | Sa(2.0s) | -0.963 | 0.237 | 4.95E-08 | 2.128 | 2.54E-05 |
| | UPD | LSF | Sa(2.0s) | -0.963 | 0.237 | 4.96E-08 | 1.718 | 2.56E-05 |
| PRC-Geom1-NA-A | GC | GPP | Sa(2.0s) | 1.513 | 0.587 | 1.98E-10 | 5.641 | 0.04 |
| | UPD | ML | Sa(2.0s) | -2.375 | 0.145 | 4.12E-04 | 0.109 | 1 |
| PRC-Geom2-NA-A | GC | GPP | Sa(2.0s) | 4.296 | 0.962 | 2.45E-13 | 8.958 | 7.96E-08 |
| | UPD | ML | Sa(2.0s) | -2.385 | 0.211 | 4.69E-04 | 0.135 | 1 |
| PRC-Geom3-NA-A | GC | ML | Sa(2.0s) | -1.401 | 0.042 | 9.11E-06 | NaN | 0.90 |
| | UPD | ML | Sa(2.0s) | -2.271 | 0.172 | 3.07E-04 | 0.129 | 1 |

(Continued)

Table 8. (Continued).

| ID-building | Failure criteria | Curve fitting method | IM | η | β | λ_f | $CoV[\lambda_f]$ | LFM |
|----------------|------------------|----------------------|----------|--------|---------|-------------|------------------|----------|
| PRC-Geom4-NA-A | GC | GPP | Sa(2.0s) | -0.994 | 0.241 | 2.44E-06 | 0.801 | 1.03E-04 |
| | UPD | ML | Sa(2.0s) | -2.269 | 0.188 | 3.14E-04 | 0.131 | 1 |
| PRC-Geom1-NA-C | GC | ML | Sa(2.0s) | -0.951 | 0.046 | 7.92E-06 | NaN | 0.45 |
| | UPD | ML | Sa(2.0s) | -2.402 | 0.209 | 1.55E-03 | 0.126 | 1 |
| PRC-Geom2-NA-C | GC | ML | Sa(2.0s) | -0.939 | 0.047 | 7.50E-06 | NaN | 0.35 |
| | UPD | ML | Sa(2.0s) | -2.244 | 0.327 | 1.24E-03 | 0.168 | 1 |
| PRC-Geom3-NA-C | GC | GPP | Sa(2.0s) | -1.071 | 0.216 | 1.94E-05 | 0.610 | 0.04 |
| | UPD | ML | Sa(2.0s) | -2.266 | 0.245 | 1.14E-03 | 0.136 | 1 |
| PRC-Geom4-NA-C | GC | GPP | Sa(2.0s) | -0.970 | 0.328 | 2.03E-05 | 0.514 | 0.09 |
| | UPD | ML | Sa(2.0s) | -2.222 | 0.245 | 1.02E-03 | 0.138 | 1 |



Table 9. S buildings.

| ID-building | Failure criteria | Curve fitting method | IM | η | β | λ_r | $Cov[\lambda_r]$ | LFM |
|------------------------|------------------|----------------------|----------|--------|---------|-------------|------------------|----------|
| S-LX20-LY6-AQ-A | GC | LSF | Sa(0.5s) | 1.037 | 0.398 | 7.03E-05 | 0.136 | 0.88 |
| | UPD | LSF | Sa(0.5s) | -0.481 | 0.280 | 4.48E-05 | 0.191 | 1 |
| S-LX20-LY6-AQ-C | GC | LSF | Sa(0.5s) | 1.043 | 0.362 | 1.85E-04 | 0.114 | 0.96 |
| | UPD | LSF | Sa(0.5s) | -0.470 | 0.269 | 3.00E-03 | 0.081 | 1 |
| S-LX20-LY6-MI-A | GC | LSF | Sa(0.5s) | -0.027 | 0.179 | 2.07E-07 | 1.687 | 8.20E-16 |
| | UPD | LSF | Sa(0.5s) | -0.530 | 0.375 | 1.47E-05 | 0.518 | 0.06 |
| S-LX20-LY6-MI-C | GC | LSF | Sa(0.5s) | -0.081 | 0.131 | 1.42E-06 | 1.176 | 1.24E-14 |
| | UPD | LSF | Sa(0.5s) | -0.431 | 0.514 | 4.46E-05 | 0.390 | 0.33 |
| S-LX20-LY6-NA-A | GC | LSF | Sa(0.5s) | 1.129 | 0.231 | 4.75E-07 | 1.300 | 3.35E-04 |
| | UPD | LSF | Sa(0.5s) | -0.524 | 0.401 | 3.82E-04 | 0.165 | 0.96 |
| S-LX20-LY6-NA-C | GC | LSF | Sa(0.5s) | 1.418 | 0.368 | 2.07E-06 | 0.702 | 0.03 |
| | UPD | LSF | Sa(0.5s) | -0.634 | 0.456 | 1.87E-03 | 0.151 | 1 |
| S-LX20-LY6-PANELS-AQ-A | GC | LSF | Sa(0.5s) | 1.181 | 0.351 | 4.48E-05 | 0.191 | 0.87 |
| | UPD | LSF | Sa(0.5s) | 0.480 | 0.329 | 2.19E-04 | 0.102 | 1 |
| S-LX20-LY6-PANELS-AQ-C | GC | LSF | Sa(0.5s) | 1.592 | 0.408 | 5.72E-05 | 0.245 | 0.86 |
| | UPD | LSF | Sa(0.5s) | 0.344 | 0.385 | 7.73E-04 | 0.121 | 1 |
| S-LX20-LY6-PANELS-MI-A | GC | LSF | Sa(0.5s) | 1.741 | 0.296 | 1.72E-12 | 6.280 | 3.59E-23 |
| | UPD | LSF | Sa(0.5s) | 0.313 | 0.356 | 1.39E-07 | 1.316 | 3.91E-06 |
| S-LX20-LY6-PANELS-MI-C | GC | LSF | Sa(0.5s) | 2.793 | 0.338 | 1.01E-13 | 9.917 | 5.46E-27 |
| | UPD | LSF | Sa(0.5s) | 0.619 | 0.351 | 1.53E-07 | 1.265 | 1.01E-04 |
| S-LX20-LY6-PANELS-NA-A | GC | LSF | Sa(0.5s) | 1.728 | 0.311 | 4.37E-08 | 3.949 | 5.28E-05 |
| | UPD | LSF | Sa(0.5s) | 0.367 | 0.302 | 1.50E-05 | 0.281 | 0.47 |
| S-LX20-LY6-PANELS-NA-C | GC | LSF | Sa(0.5s) | 1.169 | 0.239 | 3.09E-06 | 0.420 | 0.04 |
| | UPD | LSF | Sa(0.5s) | 0.486 | 0.418 | 7.82E-05 | 0.279 | 0.76 |
| S-LX20-LY8-AQ-A | GC | LSF | Sa(0.5s) | 1.594 | 0.310 | 1.33E-05 | 0.218 | 0.47 |
| | UPD | LSF | Sa(0.5s) | -0.587 | 0.270 | 1.62E-03 | 0.113 | 1 |
| S-LX20-LY8-AQ-C | GC | LSF | Sa(0.5s) | 1.312 | 0.209 | 8.20E-05 | 0.100 | 0.98 |
| | UPD | LSF | Sa(0.5s) | -0.549 | 0.479 | 4.40E-03 | 0.172 | 1 |
| S-LX20-LY8-MI-A | GC | LSF | Sa(0.5s) | -0.184 | 0.160 | 4.82E-07 | 1.331 | 4.09E-16 |
| | UPD | LSF | Sa(0.5s) | -0.522 | 0.360 | 1.25E-05 | 0.683 | 0.05 |
| S-LX20-LY8-MI-C | GC | LSF | Sa(0.5s) | -0.285 | 0.108 | 3.55E-06 | 1.007 | 2.72E-13 |
| | UPD | LSF | Sa(0.5s) | -0.398 | 0.520 | 4.11E-05 | 0.358 | 0.31 |
| S-LX20-LY8-NA-A | GC | LSF | Sa(0.5s) | 1.433 | 0.229 | 1.12E-07 | 1.372 | 7.33E-08 |
| | UPD | LSF | Sa(0.5s) | -0.469 | 0.393 | 3.20E-04 | 0.159 | 1 |
| S-LX20-LY8-NA-C | GC | LSF | Sa(0.5s) | 2.192 | 0.413 | 9.76E-08 | 1.897 | 1.42E-05 |
| | UPD | LSF | Sa(0.5s) | -0.614 | 0.427 | 1.68E-03 | 0.152 | 1 |
| S-LX20-LY8-PANELS-AQ-A | GC | LSF | Sa(0.5s) | 1.740 | 0.264 | 7.66E-06 | 0.220 | 0.27 |
| | UPD | LSF | Sa(0.5s) | 0.333 | 0.400 | 3.28E-04 | 0.140 | 1 |
| S-LX20-LY8-PANELS-AQ-C | GC | LSF | Sa(0.5s) | 1.748 | 0.265 | 2.88E-05 | 0.178 | 0.86 |
| | UPD | LSF | Sa(0.5s) | 0.226 | 0.273 | 8.55E-04 | 0.094 | 1 |

(Continued)

Table 9. (Continued).

| ID-building | Failure criteria | Curve fitting method | IM | η | β | λ_r | $CoV[\lambda_r]$ | LFM |
|------------------------|------------------|----------------------|----------|--------|---------|-------------|------------------|----------|
| S-LX20-LY8-PANELS-MI-A | GC | LSF | Sa(0.5s) | 1.089 | 0.236 | 1.32E-10 | 5.149 | 2.03E-21 |
| | UPD | LSF | Sa(0.5s) | -0.248 | 0.244 | 1.22E-06 | 0.598 | 2.86E-05 |
| S-LX20-LY8-PANELS-MI-C | GC | LSF | Sa(0.5s) | 1.482 | 0.230 | 3.02E-10 | 4.330 | 1.20E-29 |
| | UPD | LSF | Sa(0.5s) | 0.437 | 0.306 | 2.67E-07 | 0.944 | 1.84E-05 |
| S-LX20-LY8-PANELS-NA-A | GC | LSF | Sa(0.5s) | 2.730 | 0.331 | 2.08E-10 | 3.860 | 6.66E-07 |
| | UPD | LSF | Sa(0.5s) | 0.354 | 0.224 | 1.19E-05 | 0.160 | 0.48 |
| S-LX20-LY8-PANELS-NA-C | GC | LSF | Sa(0.5s) | 1.856 | 0.295 | 1.97E-07 | 0.711 | 1.51E-05 |
| | UPD | LSF | Sa(0.5s) | 0.461 | 0.265 | 6.64E-05 | 0.265 | 0.82 |
| S-LX30-LY6-AQ-A | GC | LSF | Sa(1.0s) | 0.594 | 0.317 | 2.55E-05 | 0.153 | 0.69 |
| | UPD | LSF | Sa(1.0s) | -0.958 | 0.487 | 1.01E-03 | 0.171 | 1 |
| S-LX30-LY6-AQ-C | GC | LSF | Sa(1.0s) | 0.800 | 0.439 | 7.26E-05 | 0.190 | 0.85 |
| | UPD | LSF | Sa(1.0s) | -0.831 | 0.569 | 2.12E-03 | 0.185 | 1 |
| S-LX30-LY6-MI-A | GC | LSF | Sa(1.0s) | 1.013 | 0.366 | 1.02E-11 | 3.826 | 1.60E-15 |
| | UPD | LSF | Sa(1.0s) | -0.615 | 0.556 | 9.83E-07 | 3.469 | 0.02 |
| S-LX30-LY6-MI-C | GC | LSF | Sa(1.0s) | 1.346 | 0.359 | 2.94E-11 | 10.927 | 1.70E-12 |
| | UPD | LSF | Sa(1.0s) | -0.460 | 0.533 | 3.33E-06 | 2.427 | 0.06 |
| S-LX30-LY6-NA-A | GC | LSF | Sa(1.0s) | 2.135 | 0.902 | 1.20E-07 | 4.500 | 2.24E-03 |
| | UPD | LSF | Sa(1.0s) | -0.637 | 0.452 | 6.27E-05 | 0.391 | 0.70 |
| S-LX30-LY6-NA-C | GC | LSF | Sa(1.0s) | 0.489 | 0.258 | 2.09E-06 | 0.360 | 0.05 |
| | UPD | LSF | Sa(1.0s) | -0.583 | 0.551 | 3.56E-04 | 0.322 | 0.93 |
| S-LX30-LY6-PANELS-AQ-A | GC | LSF | Sa(1.0s) | 1.218 | 0.628 | 1.25E-05 | 0.293 | 0.23 |
| | UPD | LSF | Sa(1.0s) | -0.083 | 0.690 | 2.90E-04 | 0.246 | 0.90 |
| S-LX30-LY6-PANELS-AQ-C | GC | LSF | Sa(1.0s) | 0.959 | 0.404 | 4.52E-05 | 0.185 | 0.77 |
| | UPD | LSF | Sa(1.0s) | -0.060 | 0.504 | 5.07E-04 | 0.124 | 1 |
| S-LX30-LY6-PANELS-MI-A | GC | LSF | Sa(1.0s) | 8.573 | 1.176 | 9.19E-22 | 4.458 | 7.62E-17 |
| | UPD | LSF | Sa(1.0s) | 0.176 | 0.569 | 3.17E-08 | 3.100 | 1.81E-04 |
| S-LX30-LY6-PANELS-MI-C | GC | LSF | Sa(1.0s) | 2.600 | 0.558 | 3.59E-13 | 8.269 | 2.65E-12 |
| | UPD | LSF | Sa(1.0s) | 0.570 | 0.608 | 8.64E-08 | 3.297 | 9.99E-04 |
| S-LX30-LY6-PANELS-NA-A | GC | LSF | Sa(1.0s) | 2.321 | 0.625 | 8.67E-10 | 4.818 | 1.92E-03 |
| | UPD | LSF | Sa(1.0s) | 0.195 | 0.625 | 1.04E-05 | 1.848 | 0.17 |
| S-LX30-LY6-PANELS-NA-C | GC | LSF | Sa(1.0s) | 4.400 | 0.785 | 4.11E-12 | 6.502 | 4.86E-03 |
| | UPD | LSF | Sa(1.0s) | 0.223 | 0.328 | 9.32E-06 | 0.415 | 0.30 |
| S-LX30-LY8-AQ-A | GC | LSF | Sa(1.0s) | 0.656 | 0.304 | 2.08E-05 | 0.174 | 0.62 |
| | UPD | LSF | Sa(1.0s) | -1.013 | 0.505 | 1.13E-03 | 0.160 | 1 |
| S-LX30-LY8-AQ-C | GC | LSF | Sa(1.0s) | 0.686 | 0.291 | 7.22E-05 | 0.134 | 0.99 |
| | UPD | LSF | Sa(1.0s) | -1.201 | 0.646 | 4.31E-03 | 0.163 | 1 |
| S-LX30-LY8-MI-A | GC | LSF | Sa(1.0s) | 0.162 | 0.268 | 7.96E-10 | 2.975 | 1.45E-12 |
| | UPD | LSF | Sa(1.0s) | -19 | 0.268 | 1.77E-06 | 1.628 | 0.03 |
| S-LX30-LY8-MI-C | GC | LSF | Sa(1.0s) | 1.819 | 0.353 | 8.93E-13 | 7.000 | 6.20E-15 |
| | UPD | LSF | Sa(1.0s) | -0.733 | 0.397 | 3.78E-06 | 2.347 | 0.07 |

(Continued)



Table 9. (Continued).

| ID-building | Failure criteria | Curve fitting method | IM | η | β | λ_r | $CoV[\lambda_r]$ | LFM |
|------------------------|------------------|----------------------|----------------------|-----------------|----------------|----------------------|------------------|----------------------|
| S-LX30-LY8-NA-A | GC UPD | LSF LSF | Sa(1.0s) Sa(1.0s) | 1.234 -0.766 | 0.360 0.400 | 7.46E-09 7.70E-05 | 11.089 0.288 | 3.08E-04 0.82 |
| S-LX30-LY8-NA-C | GC UPD | LSF LSF | Sa(1.0s) Sa(1.0s) | 0.659 -0.716 | 0.246 0.560 | 8.81E-07 5.18E-04 | 0.673 0.284 | 0.01 0.95 |
| S-LX30-LY8-PANELS-AQ-A | GC UPD | LSF LSF | Sa(1.0s) Sa(1.0s) | 1.343 -0.203 | 0.821 0.615 | 2.06E-05 3.11E-04 | 0.572 0.208 | 0.23 0.98 |
| S-LX30-LY8-PANELS-AQ-C | GC UPD | LSF LSF | Sa(1.0s) Sa(1.0s) | 1.135 -0.108 | 0.534 0.475 | 4.10E-05 5.31E-04 | 0.300 0.137 | 0.59 1 |
| S-LX30-LY8-PANELS-MI-A | GC UPD | LSF LSF | Sa(1.0s) Sa(1.0s) | 1.908 0.203 | 0.454 0.619 | 9.70E-14 5.29E-08 | 21.603 2.931 | 5.63E-18 4.30E-04 |
| S-LX30-LY8-PANELS-MI-C | GC UPD | LSF LSF | Sa(1.0s) Sa(1.0s) | 2.325 0.923 | 0.491 0.731 | 4.55E-13 8.48E-08 | 7.356 4.651 | 4.22E-14 1.12E-03 |
| S-LX30-LY8-PANELS-NA-A | GC UPD | LSF LSF | Sa(1.0s) Sa(1.0s) | 2.020 0.363 | 0.534 0.821 | 9.73E-10 2.27E-05 | 10.657 0.948 | 1.44E-04 0.16 |
| S-LX30-LY8-PANELS-NA-C | GC UPD | LSF LSF | Sa(1.0s) Sa(1.0s) | 2.635 0.165 | 0.577 0.392 | 1.07E-09 1.63E-05 | 2.526 0.368 | 1.96E-03 0.39 |